Adult medial habenula neurons require GDNF receptor GFRα1 for synaptic stability and function

Diana Fernández-Suárez[1,2,6], Favio A. Krapacher[1], Katarzyna Pietrajtis[3], Annika Andersson[1], Lilian Kisiswa[1,4], Marco A. Diana[3], and Carlos F. Ibáñez[1,2,5,6]

[1] Department of Neuroscience, Karolinska Institute, Stockholm 17177, Sweden

[2] Department of Physiology and Life Sciences Institute, National University of Singapore, Singapore 117597, Singapore

[3] Sorbonne Université, CNRS, INSERM, Neurosciences Paris Seine – Institut de Biologie Paris Seine (NPS-IBPS), 75005 Paris, France

[4] Department of Biomedicine, Aarhus University, 8000, Aarhus C, Denmark

[5] Peking-Tsinghua Center for Life Sciences, PKU-IDG/McGovern Institute for Brain Research, Peking University School of Life Sciences and Chinese Institute for Brain Research, 100871 Beijing, China

[6] Corresponding authors: diana.fernandez.suarez@ki.se and carlos.ibanez@ki.se

Keywords: AMPA receptors, anxiety, DREADD, fear

Running title: GDNF receptor GFRα1 is required for maintenance of medial habenula synapses

Abstract

The medial habenula (mHb) is an understudied small brain nucleus linking forebrain and midbrain structures controlling anxiety and fear behaviors. The mechanisms that maintain the structural and functional integrity of mHb neurons and their synapses remain unknown. Using spatio-temporally controlled Cre-mediated recombination in adult mice, we found that the GDNF receptor alpha 1 (GFRα1) is required in adult mHb neurons for synaptic stability and function. mHb neurons express some of the highest levels of GFRα1 in the mouse brain, and acute ablation of GFRα1 results in loss of septo-habenular and habenulo-interpeduncular glutamatergic synapses, with the remaining synapses displaying reduced numbers of presynaptic vesicles. Chemo- and opto-genetic studies in mice lacking GFRα1 revealed impaired circuit connectivity, reduced AMPA receptor postsynaptic currents, and abnormally low rectification index of AMPARs, suggesting reduced Ca^{2+}-permeability. Further biochemical and proximity ligation assay studies defined the presence of GluA1/GluA2 (Ca^{2+}-impermeable) as well as GluA1/GluA4 (Ca^{2+}-permeable) AMPAR complexes in mHb neurons, as well as clear differences in the levels and association of AMPAR subunits in mHb neurons lacking GFRα1. Finally, acute loss of GFRα1 in adult mHb neurons reduced anxiety-like behavior and potentiated context-based fear responses, phenocopying the effects of lesions to septal projections to the mHb. These results uncover an unexpected function for GFRα1 in the maintenance and function of adult glutamatergic synapses, and reveal a potential new mechanism for regulating synaptic plasticity in the septo-habenulo-interpeduncular pathway and attuning of anxiety and fear behaviors.

Abbreviations

BAC: Bed nucleus of the anterior commisure

ChAT: Choline acetyltransferase

CNO: Clozapine-N-oxide

CR: Calretinin

DREADD: Designer Receptor Exclusively Activated by Designer Drug

dmHb: Dorsal medial habenula

EPSCs: Excitatory post-synaptic currents

FR: Fasciculus retroflexus

GDNF: Glial cell derived neurotrophic factor

GFRα1: Glial cell derived neurotrophic factor receptor alpha 1

IPN: Onterpeduncular nucleus

LHb: Lateral Habenula

mHb: Medial habenula

NCAM: Neural cell adhesión molecule

PLA: Proximity ligation assay

SNpc: Substantia nigra pars compacta

SP: Substance P

TS: Triangular septum

VGAT: Vesicular GABA transporter

VGlut1: Vesicular glutamate transporter 1

VGlut2: Vesicular glutamate transporter 2

vmHb: ventral medial habenula

VTA: Ventral tegmental área

Introduction

The habenula is a phylogenetically conserved brain structure, present in all vertebrates, consisting of two small nuclei located above the thalamus, close to the midline. Due to its distinct location and connectivity, it is thought to function as a node linking more recently evolved forebrain structures involved in executive functions with ancient midbrain areas that process aversion and reward (1). Lesions to the habenula affect different behaviors related to stress, fear, aversion, anxiety, pain and sleep (2–5). In mammals, the habenula is subdivided into two distinct subnuclei, the lateral (LHb) and medial (mHb) habenula, that present different neurochemical properties, connectivity and functions (1). In the fasciculus retroflexus (FR), one of the longest major fiber tracts in the brain and among the first to form during development, afferent axons from the two subnuclei are segregated, with LHb axons in the periphery, innervating different midbrain structures, and mHb axons in the center, all terminating in the interpeduncular nucleus (IPN) (1). Perhaps due to its prominent connections to dopaminergic and serotoninergic neurons in ventral tegmental area (VTA), substantia nigra pars compacta (SNpc) and raphe nuclei, the LHb has been more extensively studied than the mHb (6). However, mHb neurons display several characteristics that make them quite unique in the mammalian brain. A striking property of mHb neurons is their spontaneous pacemaking activity, which generates tonic trains of action potentials of about 2-10 Hz (7). Moreover, GABAergic inputs from the medial septum elicit excitation, rather than inhibition, in mHb neurons due to lack of the KCl co-transporter KCC2, a feature that is more common in the developing brain, but rare among adult CNS neurons (8). Similarly, GABA released by postsynaptic IPN neurons has been shown to act as a retrograde messenger on presynaptic GABA-B receptors

92 in mHb terminals to amplify glutamatergic transmission at habenulo-interpeduncular
93 synapses (5,9). Furthermore, the mHb is the only known structure in the adult brain
94 that contains functional NMDA receptor GluN1/GluN3A, through which glycine,
95 otherwise known as a major inhibitory neurotransmitter, regulates neuronal excitability
96 in mHb neurons (10). Finally, while the majority of AMPA receptors in the adult brain
97 are Ca^{2+} impermeable, inputs to the mHb from the triangular septum (TS) and bed
98 nucleus of the anterior commissure (BAC), as well as the mHb output to the IPN,
99 produce glutamatergic responses through Ca^{2+} permeable AMPA receptors (9,11).
100 Despite its unique properties and functional importance in fear and anxiety, very little
101 is known about the mechanisms that regulate the structural and functional plasticity of
102 mHb neurons and their synapses. Moreover, aside from electrophysiological
103 evidence, the molecular composition and functional importance of mHb Ca^{2+}-
104 permeable AMPA receptors remain to be established.

105 GFRα1 is the main binding receptor for GDNF (glial cell line-derived neurotrophic
106 factor). It lacks an intracellular domain and is anchored to the plasma membrane
107 through a glycosyl-phosphatidylinositol link (12). Through the action of plasma
108 membrane lipases, glycosyl-phosphatidy cleavage results in receptor shedding from
109 the cell surface, allowing GFRα1 to act on nearby cells (13,14). GFRα1 has been
110 shown to function both in conjunction with transmembrane co-receptor subunits, such
111 as the receptor tyrosine kinase RET (12) and the neural cell adhesion molecule NCAM
112 (15), as well as independently of these receptors (16). During development, GDNF
113 and GFRα1 are essential molecular determinants for neuronal survival, migration and
114 differentiation of a variety of neuronal subpopulations in the peripheral and central
115 nervous systems (17). Exogenously provided GDNF can promote survival of midbrain
116 dopaminergic neurons, both *in vitro* and in animal models of Parkinson's Disease, and

117 therefore has been tested in clinical trials for that disease (18). On the other hand,
118 endogenous GDNF appears to be dispensable for the survival of adult dopaminergic
119 neurons in mice (19). Although GFRα1 is highly expressed in several areas of the
120 adult brain, such as the septum, midbrain and habenula (20–23), its function in the
121 adult nervous system remains unknown.

122 The prominent expression of GFRα1 in the adult mHb led us to investigate its function
123 in these neurons using temporally and spatially controlled Cre-mediated inactivation
124 of the *Gfra1* gene. In this study, we report a previously unknown and essential role for
125 GFRα1 in the maintenance, integrity and function of mHb synapses in the adult
126 septum→mHb→IPN pathway. Significantly, loss of GFRα1 in the mHb resulted in
127 changes in the molecular composition of mHb AMPA receptors that reduced their Ca^{2+}
128 permeability, as well as alterations in fear and anxiety behaviors that paralleled those
129 observed after lesion of the septo-habenular pathway (4).

130 Results

131 Characterization of GFRα1 and co-receptor expression in
132 the septum→Hb→IPN pathway

133 Inspection of sections through the brain of tamoxifen-injected 3 month old mice
134 carrying a *Rosa26*^{dTOM} reporter under the control of a *Gfra1*$^{Cre\text{-}ERT2}$ allele (herein
135 referred to as *Gfra1*^{dTOM}) revealed very high dTOM signal in the mHb and the FR (Fig.
136 1A), comparable to or exceeding that observed in better known sites of GFRα1
137 expression, such as septum, SNpc or VTA (Fig, S1A). Particularly striking was the
138 intensity of dTOM signal in mHb axons of the FR and their terminals in the IPN (Figs.

139 1A and S1A). Q-PCR analysis of *Gfra1* mRNA expression in regions microdissected
140 from adult mouse brain showed highest expression in the Hb (Fig. S1B), while Western
141 blots confirmed highest expression in the IPN (Fig. S1C), most likely derived from mHb
142 axon terminals, since *Gfra1* mRNA was at background levels in this structure (Fig.
143 S1B). Expression of *Gdnf* mRNA and GDNF protein was found across a number of
144 adult brain regions, including Hb, septum and IPN (Figs. S1D, E). As GDNF is a
145 soluble, diffusible ligand, it is likely to be available to most neurons in those structures.

146 For a closer inspection of the cellular distribution of the expression of GFRα1 and its
147 co-receptors in the adult Hb, IPN and septum, we used mouse strains expressing GFP
148 from either the *Gfra1* (*Gfra1*^{GFP}) (see Methods section) or *RET* (*RET*^{GFP}) (24) loci, in
149 addition to *Gfra1*^{dTOM} mice and immunohistochemistry for endogenous GFRα1 and
150 NCAM. All neurons in the mHb were positive for *Gfra1*^{GFP}, while no GFP signal could
151 be detected in the LHb (Figs. 1B, C). *Gfra1*^{GFP} signal co-localized with choline
152 acetyltransferase (ChAT) in the ventral mHb (vmHb) (Figs. 1B, C). As it is well known,
153 substance P (SP) can be detected at very low levels in dorsal mHb (dmHb) somas
154 due to its rapid transport to axon terminal (25). In the IPN, both SP^{+} fibers, from the
155 dmHb, as well as ChAT^{+} fibers, from the vmHb, displayed strong GFP signal (Fig. 1D).
156 GFRα1 immunohistochemistry confirmed strong expression in the somas of adult mHb
157 neurons and their axons throughout the IPN (Fig. 1E). To assess GFRα1 expression
158 in the GABAergic IPN neurons, we used *R1CG* mice, expressing GFP from the *Gfra1*
159 locus upon Cre-mediated recombination (26), bred to *Gad67*^{Cre} mice, which express
160 Cre in GABAergic neurons (27). This revealed a small and sparse population of GFP^{+}
161 cells in the dorsal IPN which did not appear labeled for GFRα1 immunohistochemistry
162 (Fig. 1F), possibly reflecting GFP that persisted after transient expression of GFRα1
163 during development. At any rate, absence of a significant population of GFRα1

164 expressing cells in the IPN is in agreement with undetectable levels of *Gfra1* mRNA
165 in this structure (Figs. S1B, see also S3H). As for GFRα1 co-receptors, NCAM was
166 abundant in both the LHb and mHb subnuclei, overlapping with the *Gfra1*^{dTOM} signal
167 in the latter (Fig. S1F). In contrast, *RET*^{GFP} signal was only detected in the LHb, but
168 not in the mHb (Fig. S1F). Axonal projections labeled by *Gfra1*^{dTOM} and *RET*^{GFP} also
169 appeared segregated in the FR, in agreement with the peripheral localization of LHb
170 axons (28) (Fig. S1F). NCAM was detected throughout the IPN, while *RET*^{GFP} signal
171 was only observed in scattered cells localized to the dorsal portion without significant
172 overlap with mHb axons labeled by *Gfra1*^{dTOM} (Fig. S1G). In the septum, no *Gfra1*^{GFP}
173 signal could be detected in calretinin (CR)$^{+}$ neurons of the BAC or TS, the two
174 subpopulations that project to the mHb (Fig. 1G). To ascertain whether the remaining
175 *Gfra1*^{GFP} cells observed adjacent to the TS projected to the mHb, we performed
176 flourogold retrograde tracing by stereotaxic injection in the mHb, followed by
177 examination of fluorogold co-localization with *Gfra1*^{GFP} signal in the TS (Figs. S2A, B).
178 Fluorogold did not overlap with GFP in the TS, although it did with CR, as expected
179 (Figs. S2C, D), indicating that septal axons projecting to the mHb do not carry GFRα1.
180 In the TS, a sparse cell subpopulation displayed *RET*^{GFP} signal, but it did not overlap
181 with either the fluorogold tracer injected in the mHb (Figs. S2E-H), *Gfra1*^{dTOM} signal
182 (Fig. S2I), or CR (Figs. S2G,H). No *RET*^{GFP} signal could be detected in BAC (Fig.
183 S2G). Finally, NCAM was readily detected in both TS and BAC, where it decorated
184 the plasma membrane of CR^{+} projection neurons (Figs. S2J, K).

185 Next, we assessed whether GFRα1 is located at synapses in the septum→mHb→IPN
186 pathway. By Western blotting, we established the enrichment of GFRα1 and NCAM in
187 synaptosomal fractions purified from adult mHb and IPN whole tissue extracts, as
188 identified by the synaptic marker PSD95 (Figs. 1H, I). RET could not be detected in

189 mHb extracts, and was excluded from synaptosomes in the IPN, while GDNF was
190 present in whole tissue extract and cytosolic fractions of both structures (Fig. 1I). By
191 immunohistochemistry, approximately two thirds of all GFRα1^{+} puncta in the mHb and
192 in the IPN co-localized with the synaptic marker PSD93 (Figs. 1J-M), confirming a
193 predominantly synaptic location of GFRα1 in these structures. Although the resolution
194 of this analysis does not allow to determine the sub-synaptic localization of GFRα1,
195 the absence of GFRα1 from septal neurons projecting to the mHb, and from IPN
196 neurons, would indicate that GFRα1 is postsynaptic in septo-habenular synapses and
197 presynaptic in habenulo-interpeduncular synapses.

198 Adult ablation of GFRα1 induces presynaptic alterations 199 and loss of glutamatergic synapses in the mHb and IPN

200 Global ablation of GFRα1 expression in adult mice was attained by crossing *Gfra1*$^{fx/+}$
201 and *Gfra1*$^{CreERT2/+}$ strains to obtain *Gfra1*$^{+/+}$, *Gfra1*$^{CreERT2/+}$ and *Gfra1*$^{CreERT2/fx}$ animals,
202 herein referred to as WT, Het and KO, respectively. Tamoxifen treatment at 3 months
203 of age reduced GFRα1 expression to near background levels in the mHb and IPN of
204 KO mice (Figs. S3A-H). Specific ablation of GFRα1 expression in the mHb was
205 achieved by bilateral, stereotaxic injection of adeno-associated viruses (AAV2)
206 expressing CRE recombinase under the control of a CMV promoter into the mHb of 3
207 month old *Gfra1*$^{fx/fx}$ mice (herein called mHb.KO). Virus injection reduced GFRα1
208 levels by 56% and 60% in mHb and IPN, respectively, compared to mock-injected
209 animals (herein called mHb.WT) (Figs. S3I-K).

210 The numbers of synaptic puncta double-labeled by pre- and post-synaptic markers
211 Synapsin 1 and PSD93, respectively, were decreased by approximately half in both

212 mHb and IPN of KO mice compared to Het or WT 28 days after tamoxifen treatment
213 (Figs. 2A, B), suggesting loss of synapses after global ablation of GFRα1. A very
214 pronounced decrease in the number of glutamatergic puncta labeled by vesicular
215 glutamate transporters 1 and 2 (VGlut1 and VGlut2) was also observed in the mHb
216 and IPN of KO mice 28 days after tamoxifen administration (Figs. 2C, D and S4A, B).
217 In contrast, mHb synaptic puncta labeled by vesicular GABA transporter (VGAT) and
218 gephyrin, corresponding to inhibitory synapses, were not affected (Fig. S4C, D). This
219 indicated a specific loss of glutamatergic synapses in the KO mHb, which constitute
220 the main afferents from the posterior septum (11,29). Importantly, the numbers of
221 synaptic puncta labeled by Synapsin 1, PSD93, VGlut1 and VGlut2 were all
222 significantly reduced in the mHb and IPN of mHb.KO mice 28 days after Cre virus
223 injection (Figs. 2E-H), confirming the specific requirement of adult mHb GFRα1
224 expression for the maintenance of glutamatergic synapses in both the mHb and IPN.

225 Synapses in the mHb and IPN were further characterized by transmission electron
226 microscopy. In agreement with our immunohistochemistry results, the number of
227 synapses in the mHb was decreased by half in KO mice compared to Het or WT
228 animals (Fig. 3A, B). Intriguingly, a marked presynaptic phenotype was observed in
229 the remaining synapses, characterized by a reduction in the number of presynaptic
230 vesicles, which affected both KO and Het mice (Fig. 3A, B). On the other hand, the
231 postsynaptic length and the width of the synaptic cleft were not affected (Fig. 3A, B).
232 Similar defects were observed in S and crest synapses in the IPN, previously shown
233 to correspond to mHb afferents (30) (Fig. 3C, D). We note that there were no
234 differences in mHb neuron number between WT, Het and KO mice 4 weeks after
235 tamoxifen injection (Figs. S4E, F), indicating no effects on mHb neuron survival after
236 acute ablation of GFRα1 in adult mice. Together, these data indicate that adult

237 expression of GFRα1 in the mHb is essential for the maintenance of both the number
238 and structure of glutamatergic synapses in the mHb and IPN.

239 Adult loss of GFRα1 affects the functional connectivity of 240 the septum→Hb→IPN pathway and alters AMPAR-mediated 241 glutamatergic responses in mHb neurons

242 In order to assess whether adult loss of GFRα1 affects connectivity in the
243 septum→mHb→IPN pathway, we used a chemogenetic approach. In the first set of
244 experiments (Fig. 4A), an AAV2 vector containing a DREADD (Designer Receptor
245 Exclusively Activated by Designer Drug) construct driving Cre-dependent expression
246 of hM3Dq and mCherry was stereotaxically injected in the TS of WT, Het and KO mice
247 (Fig. 4A). Since the TS neurons projecting to the mHb do not express GFRα1 (i.e. no
248 Cre expression in Het or KO), a second AAV2 construct expressing both Cre and GFP
249 was delivered together with the DREADD construct. Additional control experiments
250 showed that all genotypes were infected by the AAV2 vectors with comparable
251 efficiency (Fig. S5A). Treatment with clozapine-N-oxide (CNO) for one hour resulted
252 in strong c-Fos signals in the mHb only when the DREADD construct was expressed
253 by the septal neurons (Figs. 4B and S5B). Importantly, the number of c-Fos^{+} cells was
254 significantly reduced in both Het and KO compared to WT (Fig. 4C), indicating that
255 GFRα1 is required to maintain functional connectivity in the septum-mHb pathway.

256 In the second set of experiments, the same DREADD virus was injected in the mHb,
257 while a second AAV2 virus expressing only GFP was used as control. In this case,
258 only Het and KO mice express Cre (from the *Gfra1* locus), thus in WT mice no hM3Dq
259 expression could be detected in the mHb (Fig. S5C) neither c-Fos signals in the IPN

260 after CNO treatment. c-Fos induction could neither be detected in Het or KO mice
261 when either tamoxifen or CNO were omitted (Figs. S5D, E). Treatment with CNO
262 induced strong c-Fos signals in the IPN only in the presence of the DREADD virus
263 (Figs. 4D and S5F). In this case, the number of c-Fos$^+$ cells was significantly reduced
264 in the IPN of KO mice compared to Het mice (Fig, 4E), indicating impaired connectivity
265 in the adult mHb-IPN pathway after acute loss of GFRα1.

266 The c-Fos responses observed in the mHb reflected the result of sustained
267 chemogenetic stimulation (one hour CNO treatment) of TS neurons. The decrease
268 observed in Het and KO mice is in line with their reduced number of presynaptic
269 vesicles compared to WT animals, as a smaller vesicle pool would be faster depleted
270 following prolonged activation. In order to investigate faster synaptic responses, we
271 performed electrophysiological measurements of AMPAR- and NMDAR-mediated
272 components in the mHb after optogenetic stimulation of TS afferents. AAV2 vectors
273 expressing Cre-dependent Channelrhodopsin-2 (ChR2) or Cre recombinase were
274 stereotaxically co-injected in the TS of WT, Het and KO mice (Fig. 4F). Brain slices
275 containing the mHb were prepared from 3 weeks after tamoxifen treatment, and
276 excitatory post-synaptic currents (EPSCs) elicited by optogenetic stimulation of TS
277 terminals were recorded in voltage-clamped mHb neurons. These EPSCs could be
278 completely blocked by the AMPAR and NMDAR antagonists NBQX and D-APV,
279 respectively, (data not shown), indicating that they were purely glutamatergic, in
280 agreement with previous studies (11). We found that the amplitude of AMPAR-
281 mediated EPSCs recorded at -60mV in the presence of the NMDAR antagonist D-APV
282 was significantly reduced in mHb neurons of KO mice compared to WT (Fig. 4G). On
283 the other hand, no difference between genotypes could be found in EPSCs recorded
284 at +50mV (Fig. 4H). As a result, the ratio between EPSCs amplitudes measured at

285 these two voltages, which constitutes the rectification index (R.I.) of the AMPAR
286 component of these EPSCs, was significantly lower in mHb KO neurons compared to
287 WT neurons (Fig. 4I). Neither AMPAR-mediated EPSCs amplitude nor R.I. of Het
288 neurons were significantly different from WT (Figs. 4G-I). Importantly, NMDAR-
289 mediated EPSCs were not altered in KO mHb neurons (Fig. 4J). Neither the dynamic
290 behavior of the synapses in response to trains of 10 stimulations at frequencies
291 ranging from 1 to 40 Hz was different between KO and WT mHb neurons (Figs. 4K-
292 M), suggesting that the differences observed between genotypes in EPSCs amplitude
293 were due to postsynaptic alterations. We note that the presence of rectifying AMPAR-
294 mediated EPSCs (Fig. 4I) is evidence of the existence of Ca^{2+}-permeable AMPARs in
295 mHb neurons, in agreement with previous observations (Otsu et al., 2018). Thus, the
296 lower R.I. value of AMPAR-mediated EPSCs in KO mHb neurons indicated reduced
297 Ca^{2+} permeability of AMPAR complexes in mHb neurons upon removal of GFRα1,
298 suggesting possible changes in the composition of postsynaptic AMPAR subunits in
299 these neurons.

300 Altered molecular composition of AMPAR complexes in 301 mHb neurons after adult ablation of GFRα1

302 AMPAR are tetrameric ion channels formed by dimers of dimers derived from any of
303 four different subunits, termed GluA1 to 4, in different combinations (31). In the adult
304 brain, the majority of AMPAR complexes contain GluA2 subunits that have undergone
305 RNA editing, making the assembled channel Ca^{+2}-impermeable (32). On the other
306 hand, AMPAR lacking GluA2 are Ca^{+2}-permeable and, although very abundant in the
307 developing CNS, they are not common in the adult (31). Although earlier
308 electrophysiological data have indicated the presence of Ca^{2+}-permeable AMPAR

309 complexes in the septo-habenular-interpeduncular pathway (9,11), the molecular
310 composition and functional importance of these complexes are unknown.
311 Immunohistochemistry for each of the four GluA subunits in the mHb of adult WT mice
312 revealed high levels of GluA1 and GluA4, lower expression of GluA2, and negligible
313 expression of GluA3 (Fig. S6A). In the IPN, all GluA subunits were present, with
314 surprisingly high levels of GluA4 (Fig. S6A). Western-blot analysis of whole tissue,
315 cytosolic and synaptic fractions of the mHb and IPN revealed the presence of all four
316 subunits in both structures (Fig. S6B). While the GluA3 blot had to be overexposed to
317 detect specific signals, GluA4 was again very highly expressed in the IPN (Fig. S6B).
318 To better understand the composition of AMPAR complexes in the mHb and IPN, the
319 Proximity Ligation Assay (PLA) was used to investigate interactions *in situ* between
320 GluA1 and GluA2 subunits, the most common Ca^{+2}-impermeable channels in the
321 brain, and between GluA1 and GluA4, forming Ca^{+2}-permeable complexes. Both types
322 of complexes were equally present in the dorsal and the ventral portions of the mHb
323 (Figs. S6C, D), while in the IPN the lateral subnuclei presented less GluA1/GluA2 and
324 GluA1/GluA4 complexes than the core IPN (Figs. S6C, E).

325 Having established the presence of both GluA1/GluA2 (Ca^{2+}-impermeable) as well as
326 GluA1/GluA4 (Ca^{2+}-permeable) AMPAR complexes in mHb and IPN, we examined
327 possible changes in the levels, arrangement and phosphorylation state of these
328 subunits upon removal of GFRα1, as any of these can lead to changes in synaptic
329 strength and function (33). In the mHb, the level of GluA2 was significantly increased
330 in KO mice (Fig. 5A), while in the IPN, both GluA1 and GluA4 levels were reduced in
331 mice lacking GFRα1 (Fig. 5B). No statistically significant changes were observed in
332 Het mice. Whereas GluA1 phosphorylation at Ser^{831} was unchanged in the mutants,
333 phosphorylation at Ser^{845} was reduced in the mHb of KO mice (Figs. 5C-F).

334 Phosphorylation at Ser^{845} has been implicated in the insertion of GluA1 into synapses
335 (34). Changes in the composition of AMPAR complexes were evaluated by PLA.
336 GluA1/GluA2 interactions were found to be significantly increased in the mHb and core
337 IPN of KO mice (Figs. 5G, H), while GluA1/GluA4 complexes were decreased in the
338 core IPN of the mutants (Figs. 5I, J), indicating that adult loss of GFRα1 leads to
339 rearrangements in the composition of postsynaptic AMPAR subunits in the septo-
340 habenular-interpeduncular pathway which are consistent with the reduced Ca^{2+}
341 permeability of those channels.

342 Acute loss of GFRα1 in adult mHb neurons reduces anxiety-
343 like behavior and potentiates context-based fear responses

344 Selective lesion of the TS and BAC projections to the mHb has been shown to increase
345 fear responses to electric shock while decreasing anxiety-like behavior (4). We
346 performed a battery of behavioral tests 2 weeks after tamoxifen administration in WT,
347 Het and KO mice or 2 weeks after Cre virus injection in mHb.KO mice. The open field
348 and elevated plus maze were used to evaluate anxiety; foot shock-induced freezing
349 behavior, to evaluate innate fear responses; and passive avoidance and fear
350 conditioning, to evaluate fear-based learning. General locomotor activity in the open
351 field was unchanged among genotypes, although KO mice showed a trend towards
352 increased distance and time spent in the center of the arena, which did not reach
353 statistical significance (Fig. S7A). In the elevated plus maze, KO mice entered more
354 times and spent significantly longer time in the open arms than WT and Het animals,
355 suggesting reduced anxiety-like behavior in adult mice lacking GFRα1 (Fig. 6A).
356 Importantly, similar results were obtained in mHb.KO mice after Cre virus injection to
357 the mHb (Fig. S7B and Fig. 6B), indicating that GFRα1 is required in the adult mHb

358 for normal anxiety-like behaviour.

359 Freezing responses after three consecutive foot shocks were similar between WT, Het
360 and KO mice (Fig. S7C) as well as mHb.KO and mHb.WT animals (Fig. S7D),
361 indicating unaltered innate fear behavior in this test after loss of GFRα1. In the passive
362 avoidance test (Fig. 6C), both global (KO) and mHb-specific (mHb.KO) ablation of
363 GFRα1 significantly increased the avoidance latency (Figs. 6D, E), indicating
364 potentiated responses to fear-based learning after acute loss of habenular GFRα1. To
365 assess fear conditioning, mice were trained to pair a foot-shock with either a specific
366 context (Fig. 6F) or a tone cue (Fig. S7E). In the context fear conditioning, there were
367 no differences between the WT, Het and KO groups (Fig. 6G), but mHb.KO mice
368 lacking GFRα1 only in mHb neurons showed an exacerbated freezing response after
369 conditioning compared to mHb.WT controls (Fig. 6H). Finally, cued conditioned fear
370 responses did not differ between WT, Het and KO mice, or between mHb.KO and
371 mHb.WT mice (Figs. S7F, G). Together, the results of these studies show that context-
372 conditioned fear responses are significantly enhanced after acute loss of GFRα1 in
373 adult mHb neurons.

374 Discussion

375 Fear is an evolutionary conserved, adaptive behavior that helps organisms to react to
376 threatening or otherwise dangerous situations. On the other hand, persistent or
377 exaggerated fear in the absence of danger is detrimental and maladaptive. Previous
378 research has shown that neurons in the mHb play a critical role in calibrating
379 behavioral responses to threatening situations in an experience-dependent manner
380 (4,5). mHb neurons display a number of features that set them apart from the majority

381 of neurons in the adult brain, including excitatory GABAergic inputs and Ca^{2+}-
382 permeable AMPA receptors. However, the mechanisms that maintain and regulate the
383 unique properties of mHb neurons and their function in mediating fear responses
384 remain incompletely understood. Here, we demonstrate that the neurotrophic receptor
385 GFRα1 regulates synapse homeostasis in adult mHb neurons to facilitate the normal
386 processing of fear behavior. We report three major findings. First, GFRα1 is highly
387 abundant in adult mHb neurons and their terminals, where it is localized to synapses,
388 and required for the maintenance, structural integrity and function of septo-habenular
389 and habenulo-interpeduncular synaptic connections. Second, GFRα1 favors the
390 expression of Ca^{2+}-permeable AMPA receptor complexes formed by the association
391 of GluA1 and GluA4 subunits, at the expense of Ca^{2+}-impermeable GluA1/GluA2
392 complexes, in adult mHb synapses. Third, acute loss of GFRα1 in adult mHb neurons
393 reduces anxiety-like behavior and potentiates context-based fear responses,
394 phenocopying the effects of lesions to mHb afferents from the posterior septum. These
395 findings establish an unexpected role for GFRα1 as a critical mediator of the stability
396 and function of glutamatergic synapses in the adult brain.

397 GDNF was originally discovered as a survival factor for midbrain dopaminergic
398 neurons and a candidate anti-Parkinson's Disease agent (35), thereafter focusing
399 research on GDNF receptors on the SNpc and VTA areas that harbor these cells.
400 More recent studies characterized other sites of GFRα1 expression in the mammalian
401 brain, particularly in GABAergic neurons of the cerebral cortex (36,37), cerebellum
402 (38,39) and olfactory bulb (40,41). Our present findings establish mHb neurons as the
403 cells that express the highest levels of GFRα1 in the adult mouse brain, higher than
404 any other known site of expression, and the first glutamatergic neurons known to
405 require this receptor for appropriate connectivity and function. Although extensively

406 studied in the developing nervous system, the functions of neurotrophic systems in
407 the adult brain are less well understood. With the possible exception of neural injury
408 and neurodegenerative disease, adult deletion of neurotrophic factors or their
409 receptors has in most cases no effect on neuron maintenance. Our discovery of the
410 requirement of GFRα1 for the structural and functional stability of mHb glutamatergic
411 synapses represents the first demonstration of a function for this receptor in mature
412 adult neurons. Despite being only expressed by mHb neurons, GFRα1 was found
413 enriched at both septo-habenular and habenulo-interpeduncular synapses,
414 suggesting both pre and post-synaptic functions. This may be possible through the
415 release of GFRα1 from the cell surface (13,14), facilitating non-cell-autonomous
416 effects across the synapse and peri-synaptic areas. In contrast to RET, expression of
417 NCAM was detected in neurons along the septum→Hb→IPN pathway, where it was
418 also concentrated at synapses, making it a possible candidate for mediating the effects
419 of GFRα1 in this circuit. NCAM has been found to contribute to several functions in
420 synapse development and maintenance beyond cell adhesion, including spine
421 formation (42), synapse maturation (43), presynaptic vesicle recycling (44), and
422 NMDA- and AMPA-mediated glutamatergic signaling (45). GDNF, the main ligand of
423 GFRα1, could also be detected in the septum, Hb and IPN, although its specific cellular
424 source, e.g. neurons or glia, remains to be established. The specific contributions, if
425 any, of NCAM and GDNF to the function of GFRα1 in the septum→Hb→IPN pathway
426 will require further investigation. On the other hand, the abundance of GFRα1 protein
427 in cell bodies and terminals of mHb neurons suggests other mechanisms may also be
428 possible, including structural roles in overall synapse stability, and regulation of
429 trafficking or turn-over of AMPAR subunits.

430 Our behavioral studies in adult mice following acute loss of GFRα1 in mHb neurons

431 revealed an unexpected requirement for this receptor in normal anxiety-like behavior
432 and conditioned fear responses. The behavioral effects observed in the mutants
433 resembled lesions to glutamatergic TS and BAC afferents to the mHb (4), indicating
434 that GFRα1 is a positive regulator of glutamatergic transmission in the
435 septum→Hb→IPN pathway, and an essential component for normal mHb neuron
436 function. The haploinsufficiency observed in HET mice for some of the phenotypes
437 indicates a dosage effect, and suggests a potential mechanism for adjusting the
438 functional response of the pathway to dangerous or threatening situations by
439 regulating the levels of GFRα1, its ligands or co-receptors. In this context, it would be
440 important to identify the environmental cues and/or internal states that may affect
441 GFRα1 expression in mHb neurons, as well as its trafficking and accumulation in mHb
442 terminals. Finally, our findings open up a new avenue for investigations into the
443 functional plasticity of mHb neurons, which will not only improve our understanding of
444 psychiatric disorders associated with fear and anxiety, but also potentially lead to novel
445 treatments for such disorders.

446 Methods

447 Mice

448 Mice were housed 2-5 per cage in standard conditions in a temperature and humidity-
449 controlled environment, on a 12/12 h light/dark cycle with *ad libitum* access to food
450 and water. The following transgenic mouse lines were used for experiments: *EIIa*^{Cre}
451 (46), *Gad67*^{Cre} (27), *Gfra1*$^{Cre\text{-}ERT2}$ (38), *Gfra1*^{LoxP}(kindly provided by M. Saarma and
452 J.O Andressoo, University of Helsinki), *R1CG*^{LoxP}*,* which expresses GFP from the
453 *gfra1* locus after Cre-mediated recombination (26), *Ret*^{GFP} (24) *Rosa26*^{dTom} (47). The

454 *gfra1*^{gfp} mouse line was generated by crossing *EIIa*^{Cre} with *R1CG*^{LoxP} mice to obtain
455 GFP expression under the *Gfra1* promoter in the germ cells and subsequently crossing
456 the offspring with C57BL/6 mice. All animals were bred in a C57BL6/J background
457 (Jackson) with the exception of the *gfra1*^{LoxP} that was kept in a CD1 background
458 (Jackson). Therefore, all animals resulting from breeding *Gfra1*$^{Cre\text{-}ERT2}$ and *Gfra1*^{LoxP}
459 mice were 50:50 C57BL6/J: CD1 background. Both males and females were used for
460 these studies. Animal protocols were approved by Stockholms Norra
461 Djurförsöksetiska Nämnd and are in accordance with the ethical guidelines of
462 Karolinska Institutet (permit numbers N173-15; 11563-2018 and 11571-2018).

463 Tamoxifen treatment and stereotaxic surgery

464 Adult mice (3-4 months old) were injected intraperitoneally (i.p.) with 100 mg/kg of
465 tamoxifen (Sigma-Aldrich) dissolved in 10% EtOH in corn oil (Sigma-Aldrich) for 5
466 consecutive days. Adult mice (3-4 months old) were anesthetized with isoflurane (1-
467 5%) and placed in a stereotaxic frame (David Kopf Instruments). Injection was
468 performed with a wiretrol capillary micropipette (Drummond scientific) by nanoliter
469 pressure injection at a flow rate of 50 nL per min (Micro4 controller, World Precision
470 Instruments; Nanojector II, Drummond Scientific). The pipette was left on place for 10
471 min after the injection before retracting it slowly from the brain. *Gfra1*^{LoxP} mice were
472 injected bilaterally with 300 nL of AAV2-CMV-PI-Cre-rBG (Penn Vector Core,
473 2.27×10^{13} genomic copies per mL) or vehicle in the following coordinates obtained
474 from the Paxinos and Franklin atlas: (i) mHb (10° angle at the coordinates
475 anteroposterior AP -1.94 mm, mediolateral ML ±0.75 mm, dorsoventral DV –2.3 mm).
476 Due to the lack of a reporter gene in the viral construct, the expression levels of GFRa1
477 in the mHb were evaluated in all cases by immunofluorescence at the end of the

478 experiment and the ones showing no loss were removed from the experimental data
479 set. To evaluate the transfection efficiency of the viral vector, *R1CG*^{LoxP} mice were
480 injected with the virus in the same coordinates, observing GFP expression under the
481 *gfra1* promoter after Cre recombination.

482 Biochemical techniques

483 Tissue processing

484 Animals were sacrificed by cervical dislocation, brains were rapidly removed,
485 dissected manually, frozen in dry ice and stored at -80 °C until further use. For the
486 dissection of the mHb and the IPN, brains were cut coronally with a blade at -1mm
487 from bregma and +1mm from lambda, obtaining a coronal section containing the
488 habenula. The cortex and the hippocampus from that section were removed, leaving
489 the mHb on sight, which was dissected by pulling it out carefully. Next the IPN, which
490 could be visualized directly in the remaining caudal part of the brain, was collected.

491 RNA extraction and Real-time RT-PCR

492 The mRNA levels of *Gfra1* and *Gdnf* were quantified by real-time RT-PCR in total RNA
493 collected from the brain areas of interest relative to a geometric mean of mRNAs
494 encoding the ribosomal protein 18S. Total mRNA was isolated from the dissected
495 brain areas using the RNeasy Mini Kit (Qiagen) according to manufacturer's protocol.
496 The purity and quantity of RNA were measured in a nanodrop 1000 (ThermoScientific).
497 cDNA was synthesized by reverse transcription using 150 ng of RNA in a reaction
498 volume of 20 ul using the High Capacity cDNA reverse transcription kit (Applied
499 Biosystems) according to the manufacturer's protocol. cDNA samples were diluted 1:3

500 in H2O before used, and to measure the levels of 18S a further 2:800 dilution was
501 made. Real-time RT-PCR was conducted using the 7500 Real-Time PCR system
502 (Applied Biosystems) with SYBR Green fluorescent probes using the following
503 conditions: 40 cycles of 95°C for 15 s, 60°C for 1 min and 72°C for 30s. Forward and
504 reverse primers were ordered from Sigma and used at a concentration of 100 nM
505 each. The following primer pairs were use: gfra1 (Fw: 5´-
506 GAAGATTGCCTGAAGTTTCTGAAT-3´; Rv: 5´-GGTCACATCCGAGCCATT-3´); gdnf
507 (Fw: 5'-GTGACTCCAATATGCCTGAAGA-3'; Rv: 5'-CGCTTGTTTATCTGGTGACCT-
508 3'); 18S (Fw: 5´- CAATTATTCCCCATGAACG-3´; Rv: 5´-
509 GGCCTCACTAAACCATCCAA-3´). Five biological replicates were performed for each
510 study group. All the experiments were carried out in triplicates for each data point.
511 Data analysis was performed using the $2^{-\Delta Ct}$ method, and relative expression levels
512 were calculated for each sample after normalization against the housekeeping gene
513 18S.

514 Protein collection and Western-blot

515 The whole extract and the cytosolic and synaptosome protein fractions were collected
516 using the Syn-PER™ Synaptic Protein Extraction Reagent (ThermoFisher) following
517 manufacture instructions. The mHb and the IPN of two mice per genotype were pulled
518 together due to the small size of the nuclei of interest. Protein concentration was
519 measured with the Pierce™ BCA Protein Assay Kit (ThermoFisher) and samples were
520 prepared for SDS-PAGE (20 ug per sample) in SDS sample buffer (Life Technologies)
521 and boiled at 95°C for 10 min before electrophoresis on 4-12% pre-cast gels (Sigma)
522 following manufacture instructions. Proteins were transferred to polyvinylidene fluoride
523 (PVDF) membranes (Amersham). Membranes were blocked with 5% non-fat milk in

524 TBST and incubated with primary antibodies overnight in 1% milk. The following
525 primary antibodies were used at the indicated dilutions: Goat anti GFRα1 (1:500,
526 AF560, RnD): goat anti c-RET (1:500, AF482, RnD); rabbit anti NCAM (1:1000,
527 AB5032, Millipore); Mouse anti PSD95 (1:1000, MA1-046, Thermo Scientific); Mouse
528 anti GDNF (1:200; Sc-13147, Santa Cruz); rabbit anti GluA1 (1:1000, AB1504,
529 Millipore); rabbit anti GluA2 (1:1000, AB1768-I, Millipore); rabbit anti GluA3 (1:1000,
530 AGC-010, Alomone Labs); rabbit anti GluA4 (1:1000, AB1508, Millipore); rabbit anti
531 phospho-Ser831 GluA1 (1:500, 75574, Cell Signaling); rabbit anti phospho-Ser845
532 GluA1 (1:500, 8084, Cell Signaling); mouse anti tubulin alpha (1:10000, T6199,
533 Sigma). Immunoreactivity was visualized using appropriate horseradish peroxidase
534 (HRP)-conjugated secondary antibodies (1:5000, Dako). Immunoblots were
535 developed using the ECL Advance Western Blotting Detection kit (Life Technologies)
536 or the SuperSignal West Femto Maximum sensitivity substrate (ThermoFisher) and
537 images were acquired with the Image-Quant LAS4000 (GE Healthcare). Image
538 analysis and quantification of band intensities were done with ImageQuant software
539 (GE Healthcare).

540 Histological techniques

541 Tissue processing

542 Mice were deeply anaesthetized with isoflurane (Baxter Medical AB), and
543 transcardially perfused with 25 ml of 0.125 M phosphate buffered saline (PBS, pH 7.4,
544 Gibco) and 40 ml of 4% paraformaldehyde (PFA, Histolab Products AB). Brains were
545 removed, post fixed in PFA overnight and cryoprotected in 30% sucrose in PBS. To
546 obtain 20 µm floating sections, brains were embedded in OCT compound (Sakura),

547 frozen at -80°C and cut with a cryostat (CryStarNX70, ThermoScientific). To obtain 30
548 µm sections, brains were cut in a microtome (Leica SM2000 R). All sections were
549 stored at -20°C in a cryoprotective solution containing 1% DMSO (Sigma-Aldrich) and
550 20% glycerol (Sigma-Aldrich) in 0.05M Tris-HCl pH 7.4 (Sigma-Aldrich).

551 General immunofluorescence

552 30 µm brain sections were washed in PBS and blocked for 1 h in 5% normal donkey
553 serum (NDS, Jackson Immunoresearch) and 0.3% Triton X-100 (Sigma-Aldrich) in
554 PBS. Incubation with the primary antibodies was done overnight at 4°C in blocking
555 solution. After 3x10 min washes with PBS, the sections were incubated with the
556 corresponding secondary donkey Alexa fluorescent antibodies (1:1000,
557 ThermoFisher) and 0.1 mg/ml of 40-6-diamidino-2-phenylindole (DAPI; Sigma-Aldrich)
558 for 2h at RT. Sections were finally washed with PBS 3x10 minutes, mounted on glass
559 slides in a 0.2% solution of gelatin (Sigma-Aldrich) in 0.05M Tris-HCl buffer (pH 7.4),
560 dried and cover slipped in DAKO fluorescent mounting medium. The primary
561 antibodies used in this study were: Goat anti GFRα1 (1:500, AF560, RnD); Goat anti
562 ChAT (1:500, AP144P, Millipore); Chicken anti GFP (1:500, ab13970, Abcam); rabbit
563 anti NCAM (1:1000, AB5032, Millipore); rabbit anti cFOS (1:500, sc-52, Santa Cruz);
564 rabbit anti calretinin (1:500, AB5054, Chemicon); mouse anti calretinin (1:500, 6B3,
565 SWANT); rabbit anti GluA1 (1:500, AB1504, Millipore); rabbit anti GluA2 (1:500,
566 AB1768-I, Millipore); rabbit anti GluA3 (1:500, AGC-010, Alomone Labs); rabbit anti
567 GluA4 (1:500, AB1508, Millipore); rat anti substance P (1:500, Millipore, MAB356).

568 Retrograde tracing

569 300 nL of fluorogold (Fluorochrome) were injected unilaterally in the mHb of *Gfra1*^{GFP}

570 and *Ret*^{GFP} adult mice at the following coordinates obtained from the Paxinos and
571 Franklin atlas: 10° angle, AP -1.94 mm, ML +0.75 mm, dorsoventral DV –2.3 mm. Mice
572 were perfused 2 weeks later.

573 Immunofluorescence for synaptic markers

574 20 µm brain sections were washed in PBS, blocked for 1hr at RT in 20% NDS in PBS,
575 incubated with the primary antibodies at 4°C overnight in a solution containing 10%
576 NDS and 0.3% TX-100, washed 3x1hr in PBS, incubated in the same solution as the
577 primary antibodies with the corresponding secondary donkey Alexa fluorescent
578 antibodies (1:1000, ThermoFisher) for 2hr, washed 3x1hr in PBS, counterstained with
579 DAPI for 10 min and washed for 2x30 min in PBS. Sections were finally mounted on
580 glass slides in a 0.2% solution of gelatin (Sigma-Aldrich) in 0.05M Tris-HCl buffer (pH
581 7.4), dried and cover slipped in DAKO fluorescent mounting medium. The primary
582 antibodies used were guinea pig anti VGlut1 (1:500, AB2251, Millipore); Mouse anti
583 VGlut2 (1:500, 135421, SYSY); rabbit anti PSD93 (1:500, 124102, SYSY); Goat anti
584 GFRα1 (1:500, AF560, RnD); guinea pig anti VGAT (1:500, 131004, SYSY); Mouse
585 anti gephyrin (1:500, 147111, SYSY); goat anti synapsin Ia/b (1:500, sc8295, Santa
586 Cruz).

587 Proximity ligation assay (PLA)

588 PLA was performed according to manufacturer's instructions (Duolink; Sigma-Aldrich).
589 Briefly, 30 µm coronal sections containing the mHb and the IPN were blocked and
590 permeabilized in 5% NDS and 0.3% TX-100 in PBS for 1h and incubated with rabbit
591 anti GluA1 (1:400, AB1504, Millipore) and mouse anti GluA2 (1:400, Abcam,
592 ab192760) or rabbit anti GluA1 (1:400, AB1504, Millipore) and goat anti GluA4 (1:400,

593 ab115322, Abcam) overnight at 4°C. Mouse anti NMDAR2B (1:400, 610416, BD) and
594 mouse anti DARP32 (1:400, sc-271111, Santa Cruz) were used as negative controls.
595 Then sections were washed with PBS, incubated with minus and plus PLA probes for
596 1 hr at 37°C, washed with buffer A, incubated with Ligation-Ligase solution for 30 min
597 at 37°C, washed again with buffer A, and finally incubated with the Amplification-
598 Polymerase solution (Duolink™ In Situ detection reagents Orange) for 100 min at
599 37°C. After washing with buffer B, sections were incubated for 10 min with DAPI
600 (1:10000 in buffer B), mounted on glass slides and coverslipped with DAKO mounting
601 media.

602 Image acquisition and analysis

603 All fluorescent images were captured with a Carl Zeiss LSM 710 confocal microscope
604 using ZEN2009 software (Carl Zeiss). All images from the same brain area and
605 experiment were acquired using the same parameters. For imaging of the mHb and
606 the IPN, one section every 120um was used for all experiments (6-8 sections per mHb
607 and 4-5 sections per IPN). For the synaptic markers and the PLA experiments, 4 mHb
608 images were obtained with the 63X objective per section (one dorsal and one ventral
609 per mHb). For the IPN, 6 images were obtained per section (two dorsal, two ventral
610 and two lateral). Image analysis was made with ImageJ and Fiji softwares.
611 Quantification of the number of synaptic puncta and PLA dots was done in imageJ
612 with the plugin synaptic puncta analyzer (48). In brief, background was subtracted
613 from the image and the same intensity threshold and range of particle size was used
614 to analyze all images from the same experiment.

615 Transmission electron microscopy

616 *Gfra1*$^{+/+}$, *Gfra1*$^{CreERT2/+}$ and *Gfra1*$^{Cre/fx}$ 3-months old mice were treated with tamoxifen
617 and perfused one month later with 2.5% glutaraldehyde and 1% Paraformaldehyde in
618 0.1M PB. Brains were removed and left on the same fixative overnight at 4°C. The day
619 after 300 μm slices were obtained in a vibratome (Leica VT1000S) and the area
620 corresponding to the mHb and the IPN were cut out. Subsequent tissue preparation
621 and image acquisition was done at the electron microscopy unit (EMil) of Karolinska
622 Institutet. The tissue blocks were washed in 0.1M PB; postfixed in 2% OsO4 in 0.1M
623 PB for 2h at 4°C and then incubated with: (i) 70% EtOH for 30 min at 4°C; (ii) 95%
624 EtOH for 30 min at 4°C; (iii) 100% EtOH with 0.5% uranil acetate for 20 min at RT; (iv)
625 acetone 2x15 min RT; (v) LX-112/acetone (1:2) for 4h at RT; (vi) LX-112/acetone (1:1)
626 overnight at RT; (vii) LX-112/acetone (1:2) for 8h at RT; (viii) LX-112 overnight at RT
627 and finally embedded in LX-112 resin at 60°C. Ultrathin sections were cut with a EM
628 UC6 (Leica) and 20 images/structure (dmHb, vmHb, IPR, IPV) from each mouse were
629 acquired using both the FEI Tecnai 12 Spirit BioTwin transmission electron
630 microscope (FEI Company, Eindhoven, The Netherlands) and the Hitachi HT7700
631 (Hitachi High-technologies) transmission electron microscope both operated at 100 kV
632 and equipped with 2kx2k Veleta CCD cameras (Olympus Soft Imaging System).

633 # Chemogenetics and Optogenetics

634 ## Chemogenetics

635 *Gfra1*$^{+/+}$, *gfra1*$^{Cre/+}$ and *gfra1*$^{Cre/fx}$ adult mice were stereotaxically injected: (i) In the
636 posterior septum with 500 nL of a 1:1 mixture of AAV2-CMV-Cre-GFP (3.7×10^{12}
637 genomic copies per mL; UNC Gene therapy vector core) and AAV2-hSyn-DIO-
638 hM3D(Gq)-mCherry (6.1×10^{12} genomic copies per mL; UNC Gene therapy vector

639 core) or the AAV2-CMV-Cre-GFP virus alone in the following coordinates obtained
640 from the Paxinos and Franklin atlas :10° angle; AP -0.1 mm, ML +0.5 mm, DV – 2.58
641 mm. (ii) Bilaterally in the mHb with 300 nL of AAV2-hSyn-DIO-hM3D(Gq)-mCherry or
642 300nL of a control AAV2-CMV-GFP virus ($5.4x10^{12}$ genomic copies per mL; UNC
643 Gene therapy vector core) at the following coordinates: 10° angle, AP -1.94 mm, ML
644 ±0.75 mm, DV –2.3 mm). One week after viral delivery animals were treated with
645 tamoxifen to induce global ablation of *Gfra1* expression. Activation of hM3Dq was
646 induced by an *i.p.* injection of clozapine-N-oxide (CNO, Tocris) dissolve in 2% DMSO
647 in NaCl 0.9% serum (Braun) 28 days after the first dose of tamoxifen, and the animals
648 were perfused 1h later.

649 **Optogenetics**

650 Ex vivo electrophysiological experiments were performed as described
651 previously (11). Briefly, adult $gfra1^{+/+}$ and $gfra1^{Cre/fx}$ mice (3-4 months old) were
652 injected with 200/300nL of a 1:1 mix of AAV2/1.EF1a.DIO.hChR2.eYFP and
653 AAV2/9.CMV.Cre (with final titers of 2.02e13 and 4.90e12 GC/mL, respectively;
654 Vector Core of the University of Pennsylvania, USA) in the posterior septum at the
655 following coordinates, from bregma: ML 0.0 mm; AP 0.13–0.2 mm; DV -2.6 mm. Mice
656 were treated with tamoxifen (4 consecutive daily *i.p.* injections, 100mg/kg) starting one
657 week after surgery. Minimum 4 weeks following the injections, slices were obtained
658 and whole-cell, voltage-clamp recordings of mHb neurons were performed at 32°C -
659 34°C in a bicarbonate-buffered saline containing (in mM): 116 NaCl, 2.5 KCl, 1.25
660 NaH_2PO_4, 26 $NaHCO_3$, 30 glucose, 1.6 $CaCl_2$, 1.5 $MgCl_2$, and 5×10^{-5} minocycline
661 (bubbled with 95% O_2, 5% CO_2), and using an intracellular solution containing (in mM):
662 135 $CsMeSO_3$, 10 TEA-Cl, 4.6 $MgCl_2$, 10 HEPES, 10 K_2-creatine phosphate, 0.5

663 EGTA, 4 Na_2-ATP, 0.4 Na_2-GTP, 0.1 spermine and 1 QX-314, pH 7.35 and mOsm
664 ~300. Excitatory postsynaptic currents (EPSCs) were elicited by brief (2 to 4 ms-long)
665 pulses of blue light provided by a 470-nm wavelength diode (Thorlabs, France)
666 coupled to the slice chamber via the epifluorescence pathway of the microscope.
667 EPSCs were recorded in the constant presence in the bath of the GABAa and glycine
668 receptor blockers SR-95501 and strychnine respectively. Drugs were bath-applied:
669 AMPAR antagonist NBQX (10μM), NMDA antagonist D-APV (50μM), SR-95501 (5μM)
670 from Tocris Bioscience, and strychnine (2μM) from Sigma-Aldrich. Acquired with an
671 EPC-10 double amplifier using the PatchMaster software (both from Heka Elektronik,
672 Germany), the recordings were sampled at 10/40KHz, filtered at 10KHz and analyzed
673 offline with custom routines written in Igor (Wavemetrics, USA). NMDAR-mediated
674 EPSCs were quantified at +50mV, as the response amplitudes at the 7 ms-post peak
675 time point, at full decay of the AMPAR component. The amplitudes of the AMPAR-
676 mediated EPSC components at the holding potentials of +50mV and -60mV were
677 measured at the peaks of the responses following bath application of the NMDA
678 antagonist APV. Their ratio is the rectification index (R.I.) of the AMPAR currents.
679 before D-APV application.

680 Behavioral studies

681 All behavioral experiments were performed between 9 am and 2 pm, under low light
682 conditions and blind to the genotype and treatment. The only sex differences found
683 were on body weight, therefore the results of both sexes were pooled together. In all
684 cases mice were acclimatized to the behavioral room for at least 20 min before testing
685 and all apparatus were cleaned with 70% ethanol between animals. Behavioral
686 evaluation started 2 weeks after the first tamoxifen injection or 2 weeks after AAV2.Cre

687 virus delivery into the mHb. The different behavioral tests were performed in the
688 following order with 4 days between each test: open field test, elevated-plus maze,
689 innate fear response, passive avoidance. In a different set of mice, the following
690 behavioral tests were performed with 7 days between each test: open field test,
691 context fear conditioning, cued fear conditioning.

692 Open field test

693 Mice were placed in the center of a 48cm x 48cm transparent acrylic box equipped
694 with lightbeam strips (TSE Actimot system) and allowed to move freely for 10 min.
695 General locomotor parameters including distance travelled, time moving and distance
696 and time spent in the center of the arena were calculated using Actimot Software.

697 Elevated-plus maze

698 The apparatus consisted of a cross-shaped maze with two open arms opposite to two
699 arms enclosed by lateral walls (70 cm x 6 cm x 40 cm) elevated 70 cm above the floor.
700 Each animal was placed in the central square (6 cm x 6 cm) facing one of the open
701 arms away from the experimenter and allowed to explore the maze for 5 min. The
702 movement of the animals was recorded using the Ethovision XT-10 tracking software
703 and the number of entries and the staying time in each of the arms were analyzed.

704 Innate fear measurement

705 The innate freezing response of the animals after a foot-shock was evaluated using a
706 TSE multiconditioning system (TSE Systems). Each animal was placed in a squared
707 behavioral arena made of plexiglass, and after 3 minutes of habituation the mouse
708 received 3 consecutive footshocks separated by 1 min intervals (0.7 mA; 1s). Animals

709 were left in the arena for 2 extra minutes and the percentage of freezing behavior
710 during each minute interval was analyzed.

711 Passive avoidance

712 The apparatus chamber used in this test was composed by two compartments (a dark
713 and an illuminated one) connected through an automatic door (TSE multiconditioning
714 system, TSE Systems). On the acquisition/conditioning day animals were place on the
715 illuminated compartment and 30 s after the door was opened. When the animals
716 crossed to the dark chamber, the door was closed and they received a mild foot-shock
717 (1s, 0.7 mA). The day after the mice were placed again on the illuminated
718 compartment, 30 s later the door was opened and the latency to enter the dark side
719 was measured with a maximum latency time of 600s.

720 Context Fear conditioning

721 Mice were exposed to context A (square box with one transparent side and three black
722 sides) for 3 min ending with a foot-shock (2s, 0.7mA). The day after, the animals were
723 exposed to the same context A for 3 min and the freezing was measured using the
724 automatic counting system in the TSE system.

725 Cued Fear conditioning

726 Mice were exposed to context A (square box with one transparent side and three black
727 sides) for 2 min and then a tone was played for 20s ending with a foot-shock (0.7mA,
728 2s). The day after the animals were placed in context B (a transparent cylinder box)
729 and after 1 min they were exposed to the same tone for 5 min. The freezing was
730 measured using the automatic counting system in the TSE system.

731 ## Statistical analysis

732 Data are expressed as mean and standard errors (s.e.m). No statistical methods were
733 used to predetermine sample sizes but our sample sizes are similar to those generally
734 used in the field. Following normality test and homogeneity variance (F-test or
735 Kolmogorov-Smirnov test with Dallal-Wilkinson-Lilliefor p value), group comparison
736 was made using a unpaired student t-test, one-way or two-way ANOVA as appropriate
737 followed by Bonferroni or Tukey's multiple comparison test for normally distributed
738 data. Mann–Whitney U test or Kruskal-Wallis followed by Dunn's multiple comparison
739 test was used on non-normal distributed data. Differences were considered significant
740 for $p < 0.05$.

741 # Acknowledgements

742 The authors would like to thank Maria Christina Sergaki and Wei Wang for technical
743 assistance during the early stages of the project; Mart Saarma and Jaan-Olle
744 Andressoo (University of Helsinki, Finland) for *Gfra1*$^{fx/fx}$ mice; Linda Thors, Emma
745 Wallet and personnel from the KMB animal facility of Karolinska Institutet for their help
746 with animal care; Ilna Eleonoora Korkala for DAPI cell counts; and all CIB Lab
747 members for comments and suggestions. Support for this research was provided by
748 grants to C.F.I. from the Swedish Research Council (2016-01538 and 2020-01923)
749 and the National Research Foundation of Singapore (R-711-000-052-281).

750 # Author contributions

751 D.F.S. performed the majority of the experimental work; F.K. performed the PLA
752 experiments; M.D. and K.P. performed the optogenetic experiments; A.A. provided

technical support for mouse genotyping as well as behavioral and histology studies; L.K. contributed to initial signaling studies; D.F.S. and C.F.I. designed the experiments and wrote the paper.

References

1. Aizawa H, Amo R, Okamoto H. Phylogeny and ontogeny of the habenular structure. Front Neurosci. 2011;5:138.

2. Agetsuma M, Aizawa H, Aoki T, Nakayama R, Takahoko M, Goto M, et al. The habenula is crucial for experience-dependent modification of fear responses in zebrafish. Nat Neurosci. 2010 Nov;13(11):1354–6.

3. Lecourtier L, Kelly PH. A conductor hidden in the orchestra? Role of the habenular complex in monoamine transmission and cognition. Neurosci Biobehav Rev. 2007;31(5):658–72.

4. Yamaguchi T, Danjo T, Pastan I, Hikida T, Nakanishi S. Distinct roles of segregated transmission of the septo-habenular pathway in anxiety and fear. Neuron. 2013 May;78(3):537–44.

5. Zhang J, Tan L, Ren Y, Liang J, Lin R, Feng Q, et al. Presynaptic Excitation via GABAB Receptors in Habenula Cholinergic Neurons Regulates Fear Memory Expression. Cell. 2016 Jul;166(3):716–28.

6. Viswanath H, Carter AQ, Baldwin PR, Molfese DL, Salas R. The medial habenula: still neglected. Front Hum Neurosci. 2013;7:931.

774 7. Kim U, Chang S-Y. Dendritic morphology, local circuitry, and intrinsic
775 electrophysiology of neurons in the rat medial and lateral habenular nuclei of
776 the epithalamus. J Comp Neurol. 2005 Mar;483(2):236–50.

777 8. Kim U, Chung L. Dual GABAergic synaptic response of fast excitation and
778 slow inhibition in the medial habenula of rat epithalamus. J Neurophysiol.
779 2007 Sep;98(3):1323–32.

780 9. Koppensteiner P, Melani R, Ninan I. A Cooperative Mechanism Involving
781 Ca(2+)-Permeable AMPA Receptors and Retrograde Activation of GABA(B)
782 Receptors in Interpeduncular Nucleus Plasticity. Cell Rep. 2017
783 Aug;20(5):1111–22.

784 10. Otsu Y, Darcq E, Pietrajtis K, Mátyás F, Schwartz E, Bessaih T, et al. Control
785 of aversion by glycine-gated GluN1/GluN3A NMDA receptors in the adult
786 medial habenula. Science. 2019 Oct;366(6462):250–4.

787 11. Otsu Y, Lecca S, Pietrajtis K, Rousseau CV, Marcaggi P, Dugué GP, et al.
788 Functional Principles of Posterior Septal Inputs to the Medial Habenula. Cell
789 Rep. 2018 Jan;22(3):693–705.

790 12. Airaksinen MS, Saarma M. The GDNF family: signalling, biological functions
791 and therapeutic value. Nat Rev Neurosci. 2002 May;3(5):383–94.

792 13. Ledda F, Paratcha G, Ibáñez CF. Target-derived GFRalpha1 as an attractive
793 guidance signal for developing sensory and sympathetic axons via activation
794 of Cdk5. Neuron. 2002 Oct;36(3):387–401.

795 14. Paratcha G, Ledda F, Baars L, Coulpier M, Besset V, Anders J, et al.

796 Released GFRalpha1 potentiates downstream signaling, neuronal survival,
797 and differentiation via a novel mechanism of recruitment of c-Ret to lipid rafts.
798 Neuron. 2001 Jan;29(1):171–84.

799 15. Paratcha G, Ledda F, Ibáñez CF. The neural cell adhesion molecule NCAM is
800 an alternative signaling receptor for GDNF family ligands. Cell. 2003
801 Jun;113(7):867–79.

802 16. Ibáñez CF, Paratcha G, Ledda F. RET-independent signaling by GDNF
803 ligands and GFRα receptors. Cell Tissue Res. 2020 Oct;382(1):71–82.

804 17. Paratcha G, Ledda F. GDNF and GFRalpha: a versatile molecular complex for
805 developing neurons. Trends Neurosci. 2008 Aug;31(8):384–91.

806 18. Ibáñez CF, Andressoo J-O. Biology of GDNF and its receptors - Relevance for
807 disorders of the central nervous system. Neurobiol Dis. 2017 Jan;97(Pt B):80–
808 9.

809 19. Kopra J, Vilenius C, Grealish S, Härma M-A, Varendi K, Lindholm J, et al.
810 GDNF is not required for catecholaminergic neuron survival in vivo. Vol. 18,
811 Nature neuroscience. 2015. p. 319–22.

812 20. Golden JP, Baloh RH, Kotzbauer PT, Lampe PA, Osborne PA, Milbrandt J, et
813 al. Expression of neurturin, GDNF, and their receptors in the adult mouse
814 CNS. J Comp Neurol. 1998 Aug;398(1):139–50.

815 21. Ortega-de San Luis C, Pascual A. Simultaneous Detection of Both GDNF and
816 GFRα1 Expression Patterns in the Mouse Central Nervous System. Front
817 Neuroanat. 2016;10:73.

818 22. Quartu M, Serra MP, Boi M, Ferretti MT, Lai ML, Del Fiacco M. Tissue
819 distribution of Ret, GFRalpha-1, GFRalpha-2 and GFRalpha-3 receptors in the
820 human brainstem at fetal, neonatal and adult age. Brain Res. 2007
821 Oct;1173:36–52.

822 23. Trupp M, Belluardo N, Funakoshi H, Ibáñez CF. Complementary and
823 overlapping expression of glial cell line-derived neurotrophic factor (GDNF), c-
824 ret proto-oncogene, and GDNF receptor-alpha indicates multiple mechanisms
825 of trophic actions in the adult rat CNS. J Neurosci. 1997 May;17(10):3554–67.

826 24. Jain S, Golden JP, Wozniak D, Pehek E, Johnson EMJ, Milbrandt J. RET is
827 dispensable for maintenance of midbrain dopaminergic neurons in adult mice.
828 J Neurosci. 2006 Oct;26(43):11230–8.

829 25. Aizawa H, Kobayashi M, Tanaka S, Fukai T, Okamoto H. Molecular
830 characterization of the subnuclei in rat habenula. J Comp Neurol. 2012
831 Dec;520(18):4051–66.

832 26. Uesaka T, Jain S, Yonemura S, Uchiyama Y, Milbrandt J, Enomoto H.
833 Conditional ablation of GFRalpha1 in postmigratory enteric neurons triggers
834 unconventional neuronal death in the colon and causes a Hirschsprung's
835 disease phenotype. Development. 2007 Jun;134(11):2171–81.

836 27. Tolu S, Avale ME, Nakatani H, Pons S, Parnaudeau S, Tronche F, et al. A
837 versatile system for the neuronal subtype specific expression of lentiviral
838 vectors. FASEB J Off Publ Fed Am Soc Exp Biol. 2010 Mar;24(3):723–30.

839 28. Schmidt ERE, Pasterkamp RJ. The molecular mechanisms controlling
840 morphogenesis and wiring of the habenula. Pharmacol Biochem Behav. 2017

841 Nov;162:29–37.

842 29. Qin C, Luo M. Neurochemical phenotypes of the afferent and efferent
843 projections of the mouse medial habenula. Neuroscience. 2009
844 Jul;161(3):827–37.

845 30. Hamill GS, Lenn NJ. Synaptic plasticity within the interpeduncular nucleus
846 after unilateral lesions of the habenula in neonatal rats. J Neurosci. 1983
847 Nov;3(11):2128–45.

848 31. Greger IH, Watson JF, Cull-Candy SG. Structural and Functional Architecture
849 of AMPA-Type Glutamate Receptors and Their Auxiliary Proteins. Neuron.
850 2017 May;94(4):713–30.

851 32. Lalanne T, Oyrer J, Farrant M, Sjöström PJ. Synapse Type-Dependent
852 Expression of Calcium-Permeable AMPA Receptors. Front Synaptic Neurosci.
853 2018;10:34.

854 33. Chater TE, Goda Y. The role of AMPA receptors in postsynaptic mechanisms
855 of synaptic plasticity. Front Cell Neurosci. 2014;8:401.

856 34. Man H-Y, Sekine-Aizawa Y, Huganir RL. Regulation of {alpha}-amino-3-
857 hydroxy-5-methyl-4-isoxazolepropionic acid receptor trafficking through PKA
858 phosphorylation of the Glu receptor 1 subunit. Proc Natl Acad Sci U S A. 2007
859 Feb;104(9):3579–84.

860 35. Lin LF, Doherty DH, Lile JD, Bektesh S, Collins F. GDNF: a glial cell line-
861 derived neurotrophic factor for midbrain dopaminergic neurons. Science. 1993
862 May;260(5111):1130–2.

863 36. Pozas E, Ibáñez CF. GDNF and GFRalpha1 promote differentiation and
864 tangential migration of cortical GABAergic neurons. Neuron. 2005
865 Mar;45(5):701–13.

866 37. Canty AJ, Dietze J, Harvey M, Enomoto H, Milbrandt J, Ibáñez CF.
867 Regionalized loss of parvalbumin interneurons in the cerebral cortex of mice
868 with deficits in GFRalpha1 signaling. J Neurosci. 2009 Aug;29(34):10695–
869 705.

870 38. Sergaki MC, Ibáñez CF. GFRα1 Regulates Purkinje Cell Migration by
871 Counteracting NCAM Function. Cell Rep. 2017 Jan;18(2):367–79.

872 39. Sergaki MC, López-Ramos JC, Stagkourakis S, Gruart A, Broberger C,
873 Delgado-García JM, et al. Compromised Survival of Cerebellar Molecular
874 Layer Interneurons Lacking GDNF Receptors GFRα1 or RET Impairs Normal
875 Cerebellar Motor Learning. Cell Rep. 2017 Jun;19(10):1977–86.

876 40. Marks C, Belluscio L, Ibáñez CF. Critical role of GFRα1 in the development
877 and function of the main olfactory system. J Neurosci. 2012
878 Nov;32(48):17306–20.

879 41. Zechel S, Fernandez-Suarez D, Ibáñez CF. Cell-autonomous role of GFRα1 in
880 the development of olfactory bulb GABAergic interneurons. Biol Open. 2018
881 May;7(5).

882 42. Kraev I, Henneberger C, Rossetti C, Conboy L, Kohler LB, Fantin M, et al. A
883 peptide mimetic targeting trans-homophilic NCAM binding sites promotes
884 spatial learning and neural plasticity in the hippocampus. PLoS One.
885 2011;6(8):e23433.

886 43. Sytnyk V, Leshchyns'ka I, Schachner M. Neural Cell Adhesion Molecules of
887 the Immunoglobulin Superfamily Regulate Synapse Formation, Maintenance,
888 and Function. Trends Neurosci. 2017 May;40(5):295–308.

889 44. Shetty A, Sytnyk V, Leshchyns'ka I, Puchkov D, Haucke V, Schachner M. The
890 neural cell adhesion molecule promotes maturation of the presynaptic
891 endocytotic machinery by switching synaptic vesicle recycling from adaptor
892 protein 3 (AP-3)- to AP-2-dependent mechanisms. J Neurosci. 2013
893 Oct;33(42):16828–45.

894 45. Senkov O, Tikhobrazova O, Dityatev A. PSA-NCAM: synaptic functions
895 mediated by its interactions with proteoglycans and glutamate receptors. Int J
896 Biochem Cell Biol. 2012 Apr;44(4):591–5.

897 46. Lakso M, Pichel JG, Gorman JR, Sauer B, Okamoto Y, Lee E, et al. Efficient in
898 vivo manipulation of mouse genomic sequences at the zygote stage. Proc Natl
899 Acad Sci U S A. 1996 Jun;93(12):5860–5.

900 47. Madisen L, Zwingman TA, Sunkin SM, Oh SW, Zariwala HA, Gu H, et al. A
901 robust and high-throughput Cre reporting and characterization system for the
902 whole mouse brain. Nat Neurosci. 2010 Jan;13(1):133–40.

903 48. Ippolito DM, Eroglu C. Quantifying synapses: an immunocytochemistry-based
904 assay to quantify synapse number. J Vis Exp. 2010 Nov;(45).
905

Figure legends

Fig 1. Characterization of GFRα1 and co-receptor expression in neurons and synapses of the septum→Hb→IPN pathway

A) dTomato epifluorescence (red) in sagittal sections of *Gfra1*^{dTOM} mouse brain injected with tamoxifen at 3 months counterstained with DAPI (blue). FR: fasciculus retroflexus; Hipp: hippocampus; HTH: hypothalamus; IPN: interpeduncular nucleus; LS: lateral septum; mHb: medial habenula; MS; medial septum; Str: striatum. Scale bar, 500µm.

B) GFP (green) and ChAT (red) immunostaining in sagittal sections of 3 month old *Gfra1*^{GFP} mouse brain counterstained with DAPI (blue). 3V: 3th ventricle; LHb: lateral habenula. Scale bar, 400µm.

C-D) GFP (green), ChAT (red) and SP (grey) immunostaining in coronal sections of the mHb (C) and IPN (D) of 3 month old *Gfra1*^{GFP} mouse brain. dmHb: dorsal medial habenula; vmHb: ventral medial habenula: dIPN: dorsal IPN, vIPN: ventral IPN; IPL: lateral IPN. Scale bars, 200µm.

E) GFRα1 immunostaining (red) in coronal sections of the mHb and IPN from 3 month old control (C57BL6/J) mouse. Scale bars, 200µm.

F) GFP (green) and GFRα1 (red) immunostaining in coronal sections through the IPN of a 3 month old *Gad67*^{Cre}*;R1CG*$^{fx/fx}$ mouse. Scale bars, 100µm (merged) and 35µm (inset).

G) GFP (green) and calretinin (CR, red) immunostaining in coronal sections of the BAC and TS from 3 month old *Gfra1*^{GFP} mouse brain counterstained with DAPI (blue). Scale bars, 100µm (BAC) and 200µm (TS).

928 H,I) Immunoblots of whole (We), cytosolic (Ct) and synaptosome (Sn) protein extracts
929 from the mHb and IPN of 3 month old C57BL6/J mice probed for GFRα1 and NCAM
930 (H) or RET, GDNF and PSD95 (I). Tubulin was probed as loading control.

931 J, L) GFRα1 (green) and PSD93 (red) immunostaining in the mHb (J) and IPN (L) of
932 3 month old C57BL6/J mice. Scale bars, 10μm (merged) and 5μm (inset).

933 K, M) Quantification (±SEM) of GFRα1, PSD93 and double-labeled puncta in mHb (K)
934 and IPN (M). N=5 mice (25-30 images per mouse).
935

936 **Fig 2. Global and mHb-specific ablation of GFRα1 induces loss of glutamatergic**
937 **synapses in mHb and IPN neurons**

938 A) Synapsin-I (green) and PSD93 (red) immunostaining in coronal sections of the mHb
939 and IPN of WT, Het and KO mice. Scale bar, 10μm.

940 B) Quantification (±SEM) of puncta with co-localized immunoreactivity for Synapsin-I
941 and PSD93 in mHb and IPN. N=4-5 mice per group (25-30 images per mouse); 1-way
942 ANOVA followed by Tukey's post-hoc test; *, P <0.05.

943 C) VGlut1 (green) immunostaining in coronal sections of the mHb and IPN of WT, Het
944 and KO mice. Scale bar, 10μm.

945 D) Quantification (±SEM) of VGlut1 puncta in mHb (K) and IPN in mHb and IPN. N=5
946 mice per group (25-30 images per mouse); 1-way ANOVA followed by Tukey's post-
947 hoc test; *, P <0.05; ***, P<0.001.

948 E, G) Synapsin-I (red), PSD93 (purple), Vglut1 (green) and Vglut2 (red)
949 immunostaining in coronal sections of the mHb (E) and IPN (G) in mHb.KO or mHb.WT

950 mice. Scale bar, 10 µm.

951 F, H) Quantification (±SEM) of immunoreactive puncta for each marker in mHb (E)
952 and IPN (G) of mHb.KO or mHb.WT mice. N=6-7 mice per group (25-30 images per
953 mouse); Student's T-test; *, P< 0.05; ****, P< 0.0001.

954

955 **Fig 3. Reduced number of synapses and presynaptic vesicles in mHb and IPN**
956 **after acute ablation of GFRα1 in adult mice**

957 A, C) Transmission electron microscopy (TEM) images of the mHb (A) and the IPN
958 (C) of WT, Het and KO mice. Scale bars, 500nm and 200nm (insets).

959 B, D) Quantification (±SEM) of synapse density, synaptic cleft width, number of
960 presynaptic vesicles and postsynaptic density (PSD) length in mHb (B) and IPN (D) of
961 WT, Het and KO mice. N=3 mice per group; 1-way ANOVA followed by Tukey's post-
962 hoc test; *, P< 0.05; **, P< 0.01; ***, P< 0.001).

963

964 **Fig 4. Adult loss of GFRα1 affects the functional connectivity of the**
965 **septum→Hb→IPN pathway and alters AMPAR-mediated glutamatergic**
966 **responses in mHb neurons**

967 A) Schematics of the chemogenetic procedures.

968 B, D) mCherry epifluorescence (red) and c-FOS (in green) immunostaining in the mHb
969 (B) and IPN (D) of WT, Het and KO mice after chemogenetic activation of TS terminals
970 (B) or mHb neurons (D) expressing hM3Dq. Scale bars, 70µm and 15 µm (insets) in
971 (B), 100µm and 25 µm (insets) in (D).

972 C, E) Quantification (±SEM) of c-FOS positive cells in mHb (C) and IPN (E) of WT, Het
973 and KO mice. N=6 (C) and N=7-12 (E) mice per group (10-14 images (C) and 5-6
974 images (E) per mouse); 1-way ANOVA followed by Tukey's multiple comparison test
975 (C) or Bonferroni's post hoc test (E); *, P< 0.05; **, P< 0.01; ***, P< 0.001.

976 F) Schematics of the optogenetics procedures.

977 G-I) EPSC average amplitudes at -60mV (G) and +50mV (H) mediated by AMPA
978 receptors after optogenetic stimulation of septal fibers recorded in the presence of
979 NMDA antagonist APV. Rectification index (I) was calculated as the ratio between the
980 EPSC amplitudes at -60mV and +50 mV. N=10-14 cells per genotype; Kruskal-Wallis
981 followed by Dunn's multiple comparison test; *, P< 0.05; ***, P< 0.001.

982 J) NMDAR-mediated EPSCs at +50mV in WT (n=9), Het (n=17) and KO (n=18) mHb
983 cells after optogenetic stimulation of the septal terminals.

984 K) AMPAR-mediated EPSCs recorded at -60mV in mHb of WT and KO mice during
985 10 consecutive optogenetic 20Hz stimulations.

986 L, M) EPSC amplitude (±SEM) (L) and its variation (M) between 1st and 10th stimulation
987 at different frequencies in mHb of WT, Het and KO mice.
988

989 **Fig 5. Altered molecular composition of AMPAR complexes in mHb neurons**
990 **after adult ablation of GFRα1**

991 A, B) Immunoblots of synaptic protein fractions from mHb (A) and IPN (B) of WT, Het
992 and KO mice probed for GluA1, 2, 3 and 4 as indicated. PSD95 was probed as loading
993 control. Quantifications (±SEM) of GluA1 to 4 levels were corrected for PSD95 levels

994 and normalized to levels in WT samples. N=10 mice per group; 1-way ANOVA analysis
995 followed by Tukey's multiple comparison test; *, P<0.05; **, P< 0.01.

996 C, E) Immunoblots of synaptic protein fractions from mHb (C) and IPN (E) of WT, Het
997 and KO mice probed for GluA1 P-Ser^{831} and P-Ser^{845} as indicated, and reported for
998 total GluA1 and Tubulin as loading controls.

999 D, F) Quantifications (±SEM) of GluA1 P-Ser^{831} and P-Ser^{845} levels in mHb (D) and
1000 IPN (F) corrected for total GluA1 levels and normalized to levels in WT samples. N=13
1001 (D) and 14-15 (F) mice per group; Student's T-test; *, P<0.05

1002 G, I) Proximity Ligation Assay (PLA) signals (red) for GluA1-GluA2 (G) and GluA1-
1003 GluA4 (I) complexes in coronal sections of mHb and IPN from WT and KO mice.
1004 Counter-staining with DAPI appears in blue. Scale bars, 20 µm.

1005 H, J) Quantification (±SEM) of PLA puncta for GluA1-GluA2 (H) and GluA1-GluA4 (J)
1006 complexes in mHb, core IPN and lateral IPN (IPL) from WT and KO mice. N=5-6 mice
1007 per group (total 24 images per group); Student's T-test; *, P<0.05.
1008

1009 **Fig 6. Acute loss of GFRα1 in adult mHb neurons reduces anxiety-like behavior**
1010 **and potentiates context-based fear responses**

1011 A, B) Total entries, time spent in open arms and open arms entries (±SEM) for WT,
1012 Het and KO mice (A) and mHb.WT and mHb.KO mice (B) in the Elevated Plus Maze
1013 test. N=10-12 mice per group; 1-way ANOVA followed by Bonferroni post-hoc test (A)
1014 and Student's t-test (B); *, P<0.05; **, P<0.01.

1015 C-E) Schematic (C) and latencies (±SEM) during training and test for WT, Het and KO

1016 mice (D) and mHb.WT and mHb.KO mice (E) in the Passive Avoidance test. N=8-12
1017 mice per group; 2-way ANOVA followed by Bonferroni post-hoc test; *, P<0.05; **,
1018 P<0.01.

1019 F-H) Schematic (F), freezing time-course and total freezing time (±SEM) for WT, Het
1020 and KO mice (G) and mHb.WT and mHb.KO mice (H) in the Context Fear Conditioning
1021 test. N=8-10 mice per group; 2-way ANOVA followed by Bonferroni post-hoc test and
1022 Student's t-test; *, P<0.05; **, P<0.01.

Figure 1

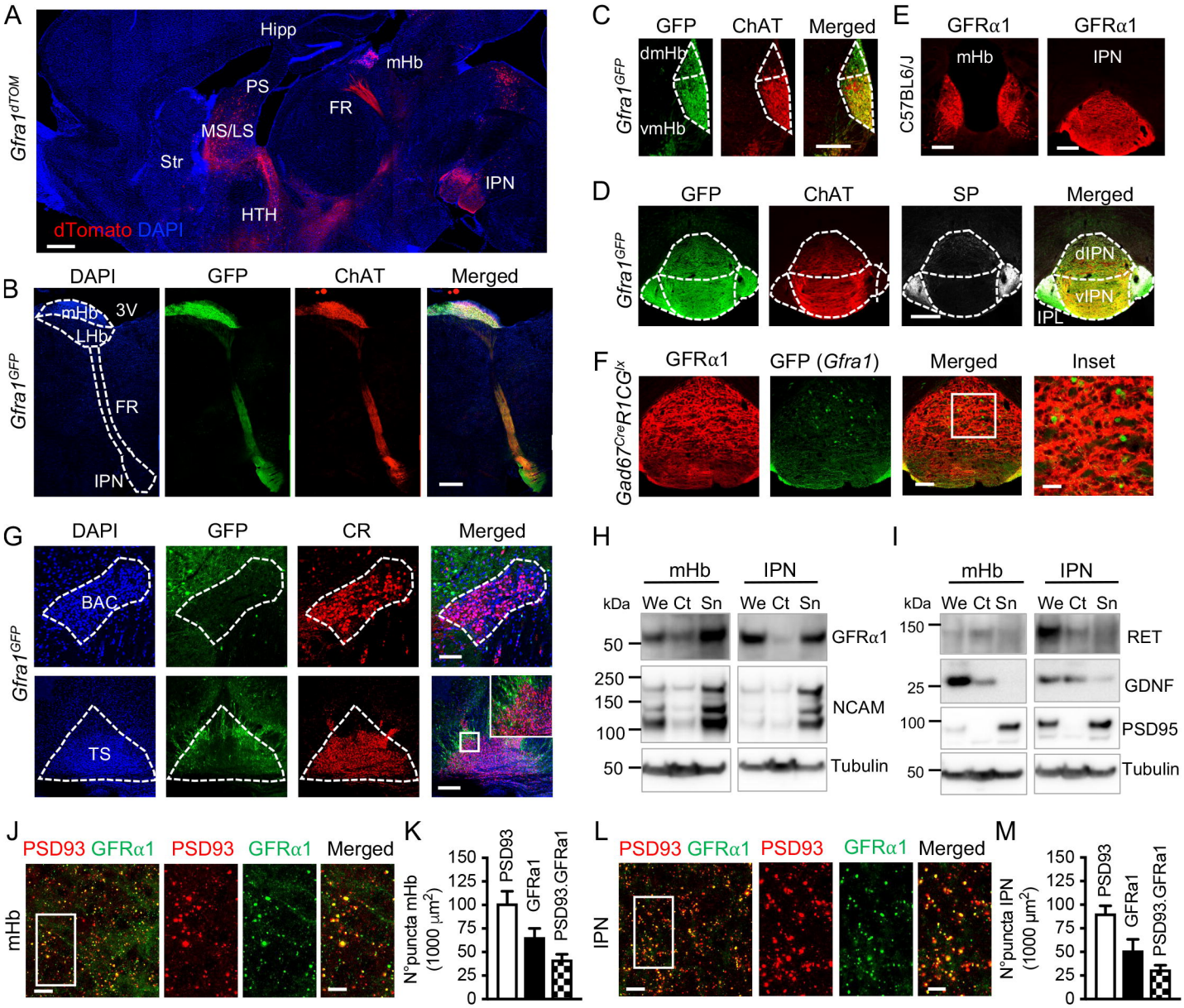
A
Gfra1dTOM
Hipp
mHb
PS
FR
MS/LS
Str
IPN
HTH
dTomato DAPI
B
DAPI
GFP
ChAT
Merged
Gfra1GFP
mHb
3V
LHb
FR
IPN
C
GFP
ChAT
Merged
Gfra1GFP
dmHb
vmHb
E
GFRα1
GFRα1
C57BL6/J
mHb
IPN
D
GFP
ChAT
SP
Merged
Gfra1GFP
dIPN
vIPN
IPL
F
GFRα1
GFP (Gfra1)
Merged
Inset
Gad67CreR1CGlx
G
DAPI
GFP
CR
Merged
Gfra1GFP
BAC
TS
H
mHb
IPN
kDa
We Ct Sn
We Ct Sn
50
GFRα1
250
150
100
NCAM
50
Tubulin
I
mHb
IPN
kDa
We Ct Sn
We Ct Sn
150
RET
25
GDNF
100
PSD95
50
Tubulin
J
PSD93 GFRα1
PSD93
GFRα1
Merged
mHb
K
N°puncta mHb (1000 μm2)
150
125
100
75
50
25
0
PSD93
GFRa1
PSD93.GFRa1
L
PSD93 GFRα1
PSD93
GFRα1
Merged
IPN
M
N°puncta IPN (1000 μm2)
150
125
100
75
50
25
0
PSD93
GFRa1
PSD93.GFRa1

Figure 2

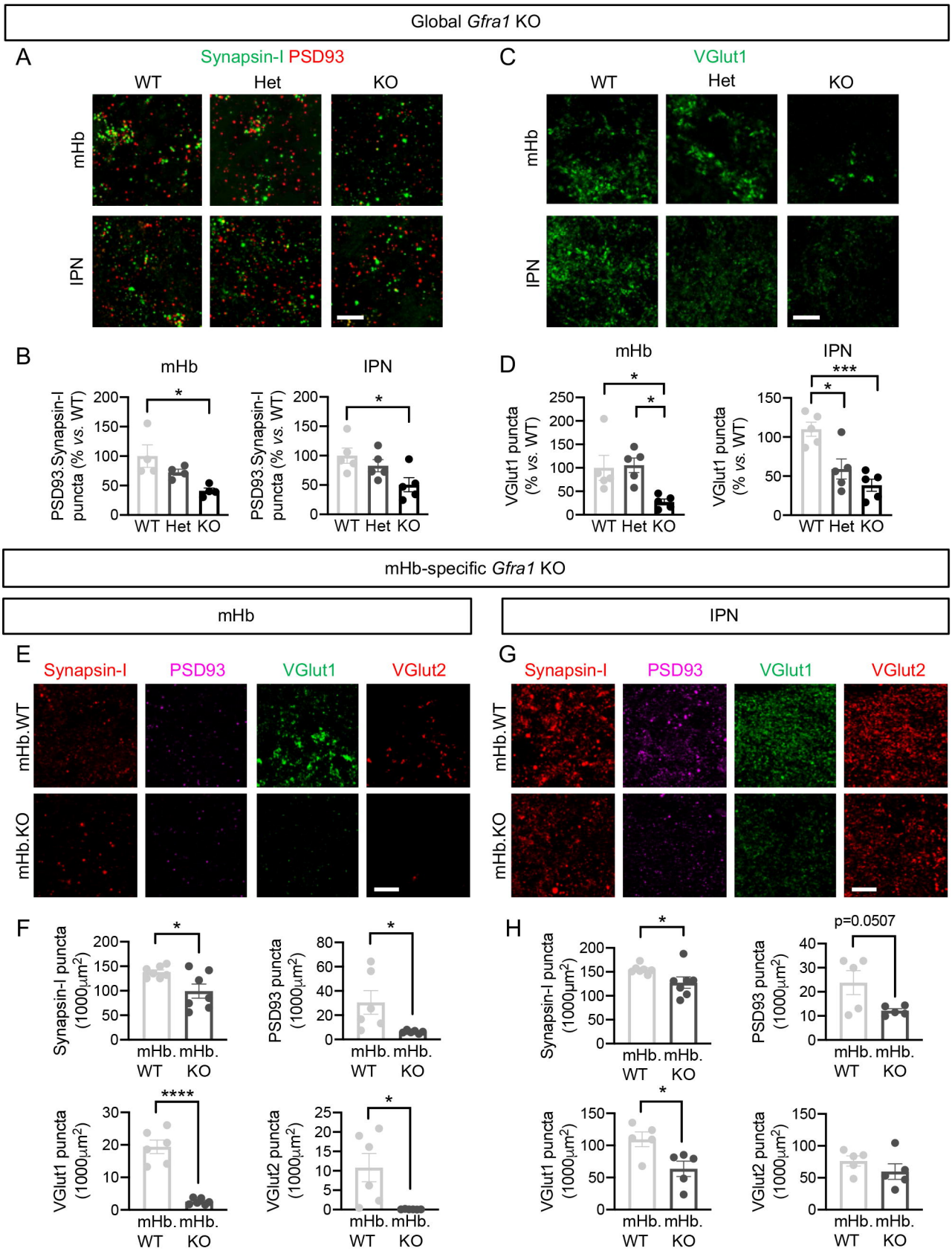
Global Gfra1 KO
A
Synapsin-I PSD93
WT
Het
KO
mHb
IPN
C
VGlut1
B
mHb
IPN
PSD93.Synapsin-I puncta (% vs. WT)
D
VGlut1 puncta (% vs. WT)
mHb-specific Gfra1 KO
mHb
IPN
E
Synapsin-I
PSD93
VGlut1
VGlut2
mHb.WT
mHb.KO
G
F
Synapsin-I puncta (1000μm²)
PSD93 puncta (1000μm²)
VGlut1 puncta (1000μm²)
VGlut2 puncta (1000μm²)
mHb. WT
mHb. KO
H
p=0.0507

Figure 3

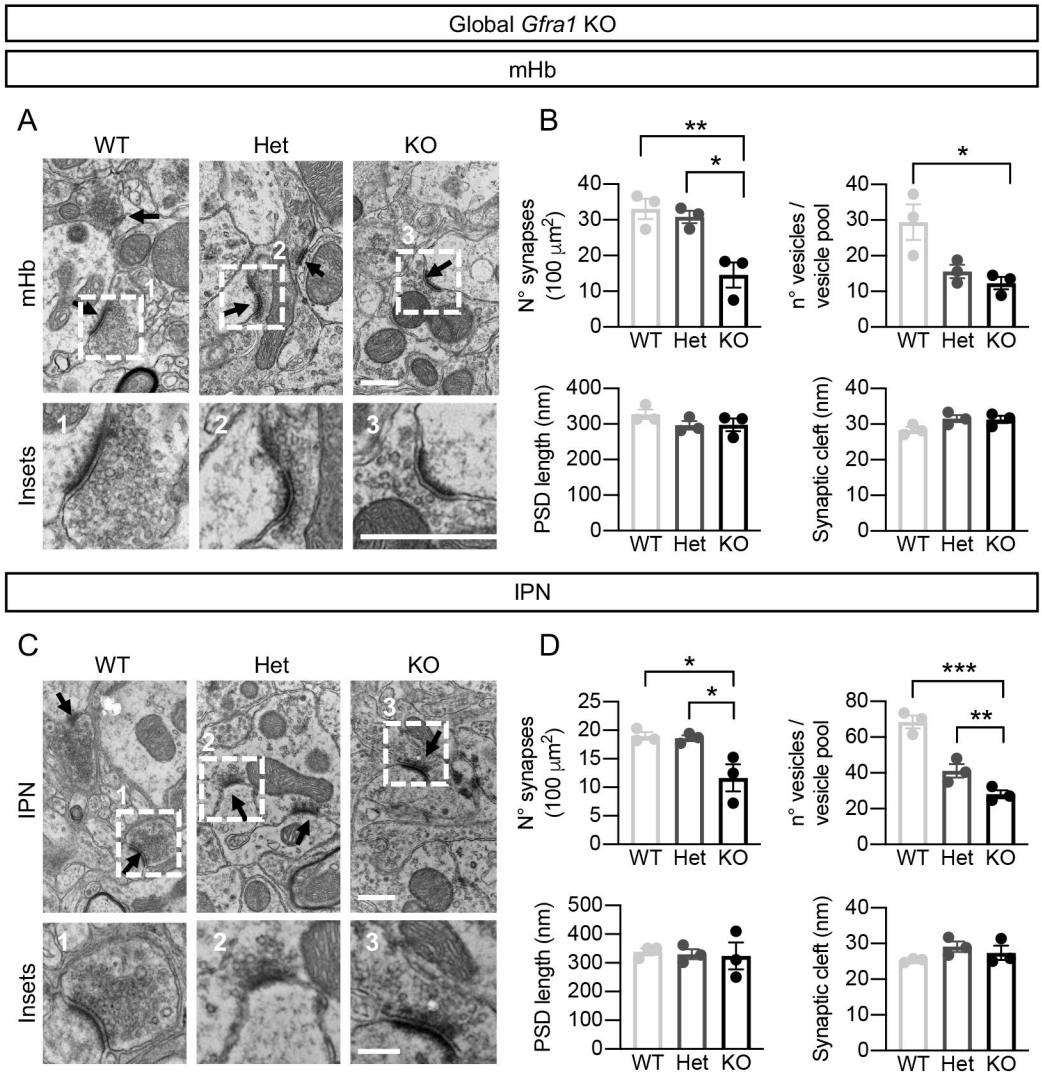
Global Gfra1 KO
mHb
A
WT
Het
KO
mHb
Insets
B
N° synapses (100 µm²)
n° vesicles / vesicle pool
PSD length (nm)
Synaptic cleft (nm)
WT Het KO
IPN
C
D

Figure 4

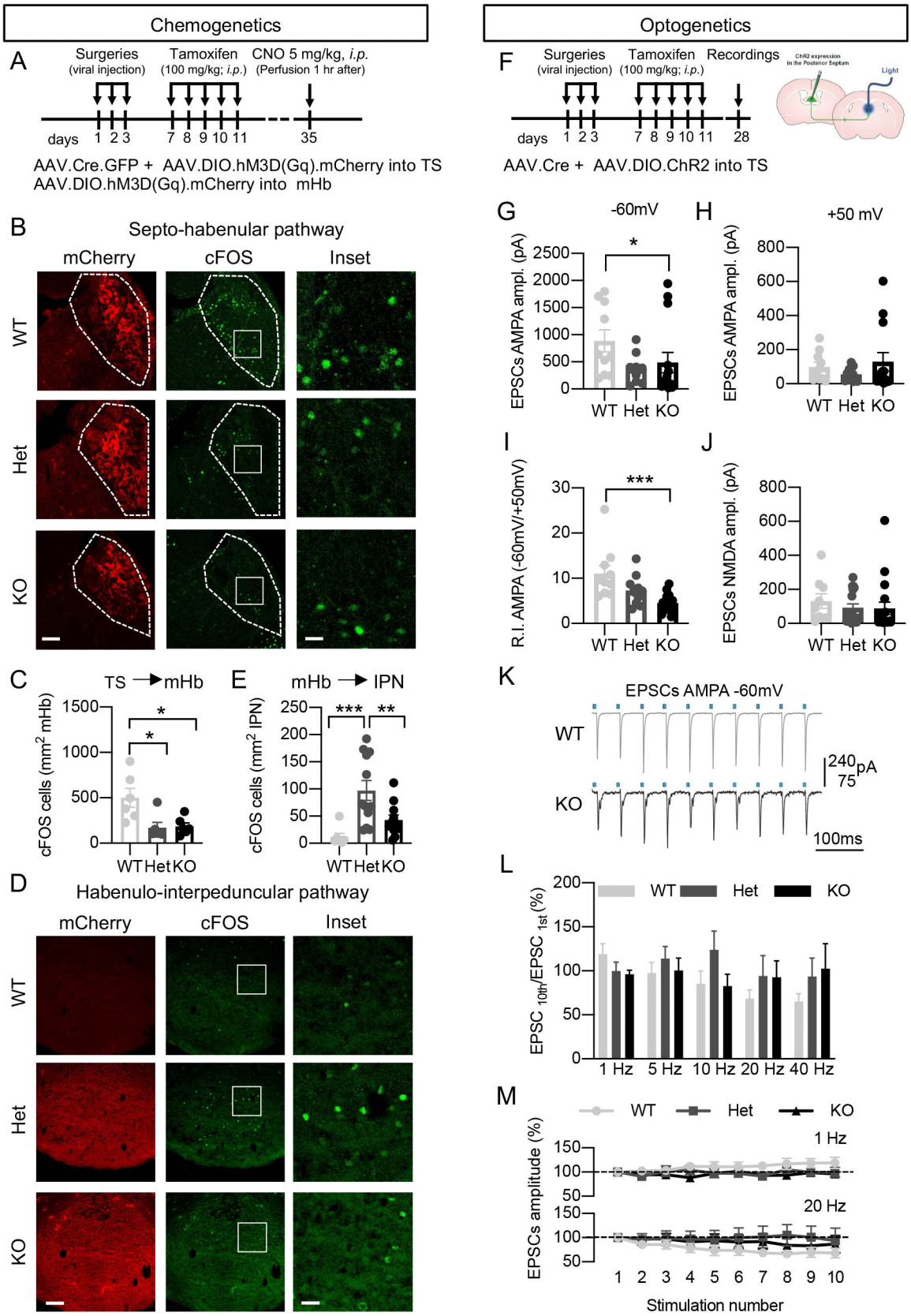
Chemogenetics
A
Surgeries (viral injection)
Tamoxifen (100 mg/kg; i.p.)
CNO 5 mg/kg, i.p. (Perfusion 1 hr after)
days 1 2 3 7 8 9 10 11 35
AAV.Cre.GFP + AAV.DIO.hM3D(Gq).mCherry into TS
AAV.DIO.hM3D(Gq).mCherry into mHb
B
Septo-habenular pathway
mCherry
cFOS
Inset
WT
Het
KO
C
TS → mHb
cFOS cells (mm2 mHb)
WT Het KO
E
mHb → IPN
cFOS cells (mm2 IPN)
WT Het KO
D
Habenulo-interpeduncular pathway
mCherry
cFOS
Inset
WT
Het
KO
Optogenetics
F
Surgeries (viral injection)
Tamoxifen (100 mg/kg; i.p.)
Recordings
days 1 2 3 7 8 9 10 11 28
Light
AAV.Cre + AAV.DIO.ChR2 into TS
G
-60mV
EPSCs AMPA ampl. (pA)
WT Het KO
H
+50 mV
EPSCs AMPA ampl. (pA)
WT Het KO
I
R.I. AMPA (-60mV/+50mV)
WT Het KO
J
EPSCs NMDA ampl. (pA)
WT Het KO
K
EPSCs AMPA -60mV
WT
KO
240 pA
75
100ms
L
WT Het KO
EPSC 10th/EPSC 1st (%)
1 Hz 5 Hz 10 Hz 20 Hz 40 Hz
M
WT Het KO
1 Hz
20 Hz
EPSCs amplitude (%)
Stimulation number

Figure 5

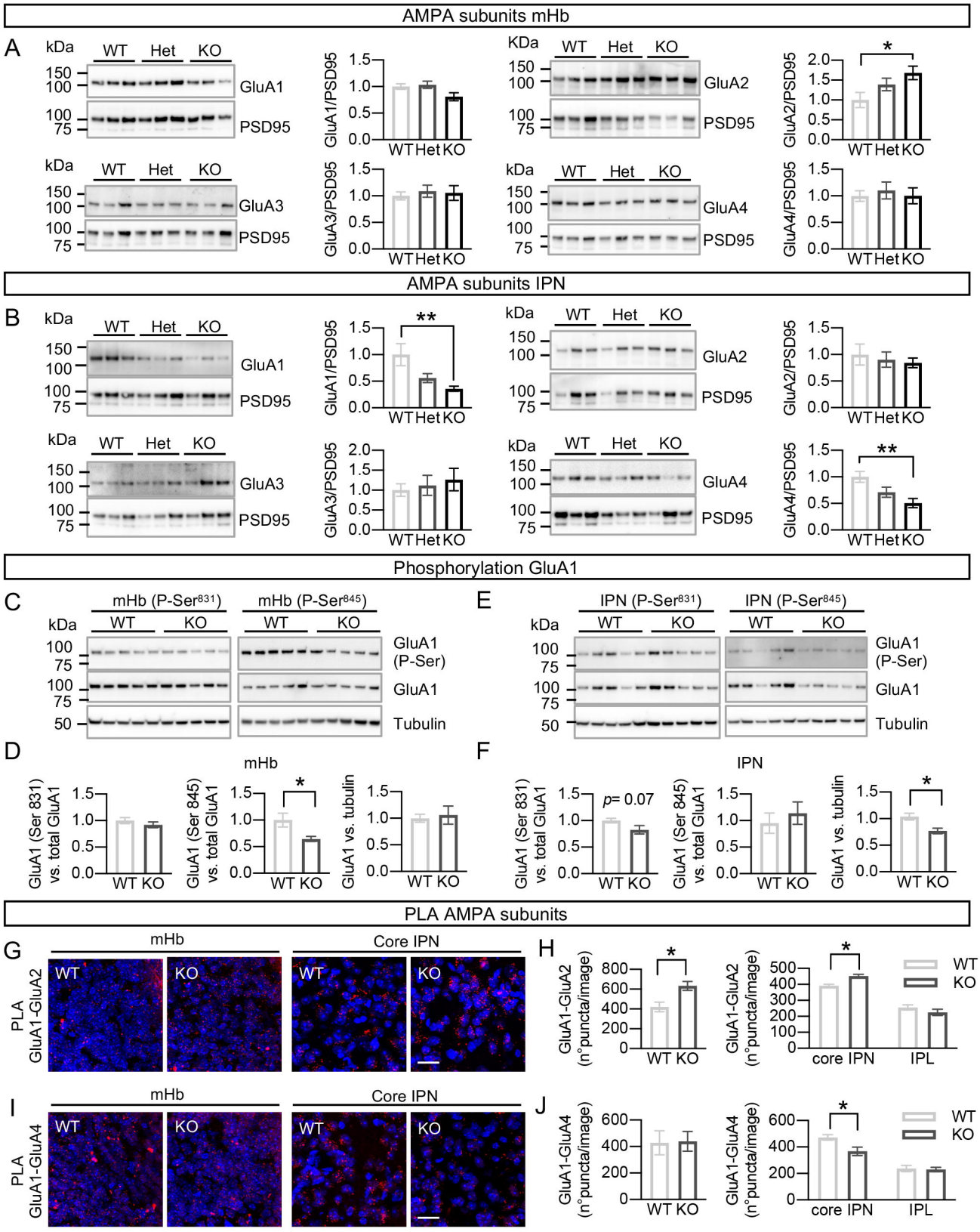
AMPA subunits mHb
A
kDa
WT Het KO
150
100
GluA1
100
75
PSD95
GluA1/PSD95
GluA2
GluA2/PSD95
GluA3
GluA3/PSD95
GluA4
GluA4/PSD95
AMPA subunits IPN
B
Phosphorylation GluA1
C
mHb (P-Ser831)
mHb (P-Ser845)
WT KO
GluA1 (P-Ser)
GluA1
Tubulin
50
D
mHb
GluA1 (Ser 831) vs. total GluA1
GluA1 (Ser 845) vs. total GluA1
GluA1 vs. tubulin
E
IPN (P-Ser831)
IPN (P-Ser845)
F
IPN
p= 0.07
PLA AMPA subunits
G
mHb
Core IPN
PLA GluA1-GluA2
H
GluA1-GluA2 (n°puncta/image)
core IPN
IPL
I
PLA GluA1-GluA4
J
GluA1-GluA4 (n°puncta/image)

Figure 6

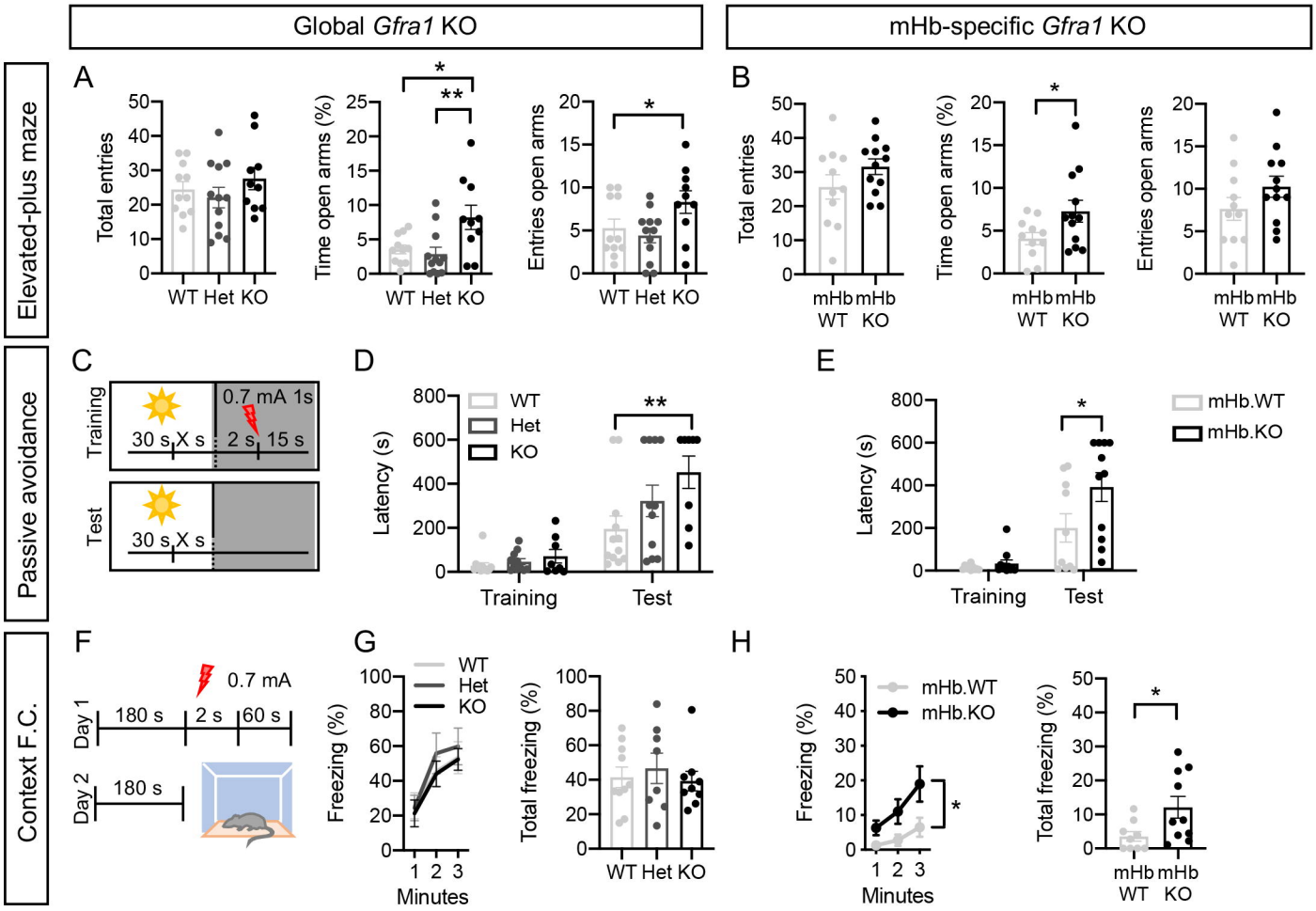
Global Gfra1 KO
mHb-specific Gfra1 KO
Elevated-plus maze
Passive avoidance
Context F.C.
A
Total entries
Time open arms (%)
Entries open arms
WT Het KO
B
mHb WT
mHb KO
C
Training
Test
30 s
X s
0.7 mA 1s
2 s
15 s
D
Latency (s)
WT
Het
KO
E
mHb.WT
mHb.KO
F
0.7 mA
Day 1
Day 2
180 s
2 s
60 s
G
Freezing (%)
Minutes
Total freezing (%)
H